Continuum Modeling and Analysis of the Frictional Interaction between a CNT and Substrate during Dragging

A Thesis Presented

by

Palaniappan Nagappan

to

Department of Mechanical and Industrial Engineering

In partial fulfillment of the requirements
for the degree of

Master of Science

in

Mechanical Engineering

in the field of

Mechanics

Northeastern University
Boston, Massachusetts

August 2008

Abstract

A simple method to determine the frictional interaction between a carbon nanotube (CNT) and a substrate is analyzed for feasibility. In this technique an atomic force microscope (AFM) tip is used to drag a CNT along a substrate. Then the deformed shape of the CNT can be viewed either with the AFM or in a Scanning Electron Microscope (SEM). An analysis of the deformed shape allows the determination of the frictional interactions which occurred during dragging. It is important to quantify these interactions in a variety of potential applications of nanotechnology. In one such example, a CNT based nanoswitch consists of a CNT bridging over a trench. Actuation of the CNT causes it to stretch and can lead to partial slip at the interface. This slip causes hysteresis which has been observed in the mechanical actuation of a CNT bridge. In this work continuum level modeling is used to determine the relationship between the shape of the CNT and the frictional interaction which occurred between the CNT and substrate during dragging. The model and analysis indicate that this method should be feasible for CNTs with aspect ratios approximately in the 100–250 range.

The modeling is extended to determine the frictional interaction between a CNT and an anisotropic substrate. Anisotropy is the property of being directionally dependent, as opposed to isotropy, which is homogeneity in all directions. In this context the shear stress offered by the substrate will vary with respect to orientation. Results of anisotropic substrate indicate the dependence of orientation of nanotube with respect to substrate and also the effect of various substrates for the same value of applied load and orientaton.

For both cases results are of high resolution if the AFM tip is away from the midpoint of the nanotube. For high values of the frictional interaction and a very long CNT there is insufficient change in the final shape of the CNT to accurately resolve the shear stress. For low values of frictional interaction CNT is apt to roll rather than slide.

Acknowledgements:

I would like to express my sincere gratitude to Professor George G Adams who advised and encouraged me during the compilation of this thesis work. Most importantly for bringing up the topic and also had been there always for those invaluable discussions.

I would also like to thank the Mechanical Engineering department for their graduate assistantship.

Last but not the least sincere appreciation to all my family and friends who had been there to encourage and help during the tough times of this study.

Table of Contents

List of Figures

Introduction

The discovery of the carbon nanotube (CNT) in 1991 by Iijima [1] has stimulated ever broader research activities in science and engineering. Their mechanical properties and structural perfection make CNTs ideal candidates for next generation electronic devices. A CNT can be imagined to be created by wrapping one or more one-atom thick graphene sheets to form a cylindrical tube structure. Thus the resulting CNT is either a single-walled nanotube (SWNT) or a multi-walled nanotube (MWNT).

It is important to quantify the frictional interactions between a CNT and various substrates. Such interactions occur in a variety of potential applications of nanotechnology. In fabrication of CNT based devices, knowledge of the interactions between CNTs and various contacting substrates is essential in order to understand the assembly processes by which these tubes are deposited. In a CNT based nanoswitch, a CNT bridges over a trench. Electrical actuation causes the tube to bend toward the electrode at the bottom of the trench. This deformation requires stretching of the CNT and/or slip at the CNT-substrate interface. The stretching is in the elastic range but interfacial slip leads to undesirable hysteresis in the switching process.

Hertel, Martel, and Avouris [2] showed that an AFM tip could be used to manipulate individual multiwalled CNTs on a passivated silicon surface. By observing the elastic distortion of a CNT over an obstacle, they were able to estimate the binding energy. Falvo et al. [3] demonstrated various manipulations of MWNTs using a specially designed nanomanipulator with a haptic interface. Their research investigated the rolling and sliding motion of carbon nanotubes using an AFM tip to push the CNTs. The force of friction was measured during both of these motions. Typically movement began as rolling and then transitioned to sliding. The nanomanipulator was further used by Falvo et al. [4] to study rolling and sliding motion of MWNTs on graphite surfaces. These tubes had aspect ratios of about 20 and the rolling was accompanied by stick-slip motion. The frictional shear stress was assumed to be constant and the measured value of approximately 2 MPa compared reasonably well with the

value of 5 MPa by Schwarz et al. [5] which was inferred from measurements of an AFM tip on graphite.

Falvo et al. [6] performed manipulation of a multi-walled CNT on a HOPG substrate. The effect of the commensurability of the surfaces on friction was investigated and found to be significant. In [7] Falvo and Superfine reviewed various studies on the mechanics and friction at the nanometer scale. The frictional sliding of a bundle of SWNTs on KCl and HOPG surfaces was reported by Miura et al. [8]. Whittaker et al. [9] presented measurements of the adhesive force between a CNT and SiO_2 substrate. The CNT spanned over two adjacent and parallel trenches. An AFM was used to push the CNT into one of the trenches, causing slip. The force required to produce slip was an indication of the CNT-substrate frictional interaction.

Hertel, Walkup and Avouris [10] investigated the effects of van der Waals forces on the deformation of a CNT on a Si surface using AFM, continuum mechanics, and molecular dynamics. They found that the radial and axial deformations experienced by a CNT on a substrate can significantly modify its ideal geometry. Pantano, Parks and Boyce [11] developed a finite element continuum model of single- and multi-walled CNTs which included van der Waals interactions. Results compared favorably with the molecular dynamics simulations in [10].

Buldum and Lu [12] conducted molecular statics and dynamics simulations of atomic scale sliding and rolling of a CNT on a graphite surface. It was shown that the effective contact area and interaction energy scale with the square-root of the radius. When the nanotube is pushed, a combination of spinning and sliding occurs. The frictional interaction between a CNT and a graphite surface was studied using molecular dynamics by Cheng and Lu [13]. It was found that the dynamic friction depends on the rotation angle of the nanotube axis with respect to the graphite surface.

This work focuses on the continuum modeling and analysis of the deformation of a CNT on a substrate, due to the CNT having been dragged along the substrate by, for example, the tip of an atomic force microscope. The shear

stress offered by the substrate while dragging the CNT is assumed to be constant along the length of the CNT. This analysis shows that the frictional interaction between the CNT and the substrate can be determined simply by observing the deformed shape of the CNT after dragging is completed. However if the aspect ratio is too large then the sensitivity of the measurement is low. If the aspect ratio is too small then the CNT is apt to roll rather than slide. Thus the results of this analysis provide an operating window for measurements. This method has the advantage of simplicity and does not require the calibration of the AFM in the lateral mode (or in any mode) as the force is not measured by the AFM.

The last part of the thesis includes analysis of frictional interaction between a CNT and an anisotropic substrate. Anisotropy is the property of being directionally dependent, as opposed to isotropy, which means homogeneity in all directions. It can be defined as a difference in a physical property (absorbance, refractive index, density, etc.) for some material when measured along different axes. In this context the shear stress offered by the substrate will vary with respect to direction.

Modeling and Analysis

The mechanical deformation model uses the theory of the elastica [14] which allows for large elastic deflections of thin structures in which the material behavior remains linear elastic. This theory will be applied to model the interaction between a carbon nanotube and a rigid substrate. Thus the nanotube is modeled using the equation of equilibrium of a bent elastic rod, the general equation for which is

$$EI\frac{d^2\psi}{d\bar{s}^2} - (T_0 - q_x\bar{s})\sin\psi - (S_0 - q_y\bar{s})\cos\psi = 0 \qquad (1)$$

As shown in Figure 1, T_0 and S_0 are the horizontal and vertical components of the internal force respectively at the origin which at that point correspond to the tension and shear force, ψ is the angle between the *x*-axis and the tangent at position $\bar{s}$ (positive clockwise), E is the elastic Young's modulus, $I = \frac{\pi}{64}D^4$ is the second moment of the cross-sectional area of diameter D of the CNT, and q_x, q_y are the components of the external load per unit length in the *x*- and *y*-directions respectively.

Two different cases were analyzed based on the point of application of the load. These configurations are symmetric loading (the force is applied at the midpoint of the CNT) and non-symmetric loading (the force is applied away from the midpoint of the CNT). In both cases, the force is applied so as to push the CNT in a direction perpendicular to its initial orientation. It is this frictional interaction which is modeled by the q_x and q_y terms in Equation (1). Implicit in our analysis is the assumption that the tube is sufficiently long so that the frictional shear stress produces enough bending to make rolling motion kinematically unfavorable. In the following analysis we show how a specified frictional interaction during sliding will cause the CNT to deform. The results of this analysis will allow us to determine the frictional interaction which occurred during dragging by observing the deformed shape of the CNT. The analysis also provides an operating window of CNT aspect ratios in which this method can be used.

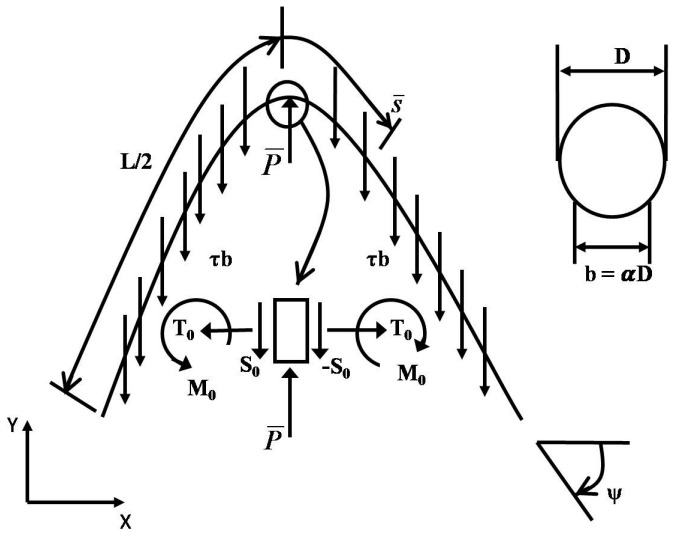

Figure 1. Schematic representation of symmetric loading of a CNT.

Symmetric Loading

This type of loading corresponds to a force applied at the midpoint of the CNT (Figure 1). The substrate on which the CNT is placed offers a shear resistance to the applied load as the CNT slides along the substrate. By rewriting Equation (1) for the symmetric case

$$EI\frac{d^2\psi}{d\bar{s}^2} - (-\frac{\bar{P}}{2} + \frac{\bar{P}}{L}\bar{s})\cos\psi = 0, \quad 0 < \bar{s} < \frac{L}{2} \tag{2}$$

is obtained. Because sliding occurs in the *y*-direction, q_x was taken to vanish and q_y was set equal to the frictional shear stress ($\bar{\tau}$) multiplied by the effective contact width (*b*). The value of *b* is somewhat arbitrarily chosen to be 0.6 times the tube diameter (*D*). However it is really only the product $\bar{\tau}b$ (the shear force per unit length or shear flow) which is important in using this result. Furthermore, by equilibrium $\bar{\tau}bL = \bar{P}$, so that knowing $\bar{\tau}bL$ is equivalent to knowing $\bar{P}$ and also $S_0 = -\bar{P}/2$ was used in Equation (1).

Since the load is applied at the midpoint, the tangent to the CNT at that point is in the x-direction. Hence one of the boundary conditions is zero rotation at the point of application of the load. The second boundary condition is that the

bending moment at the free end of the CNT is zero. These conditions are written as

$$\psi(0) = 0, \qquad EI\psi'(L/2) = 0 \tag{3}$$

where prime (′) denotes differentiation with respect to $\bar{s}$.

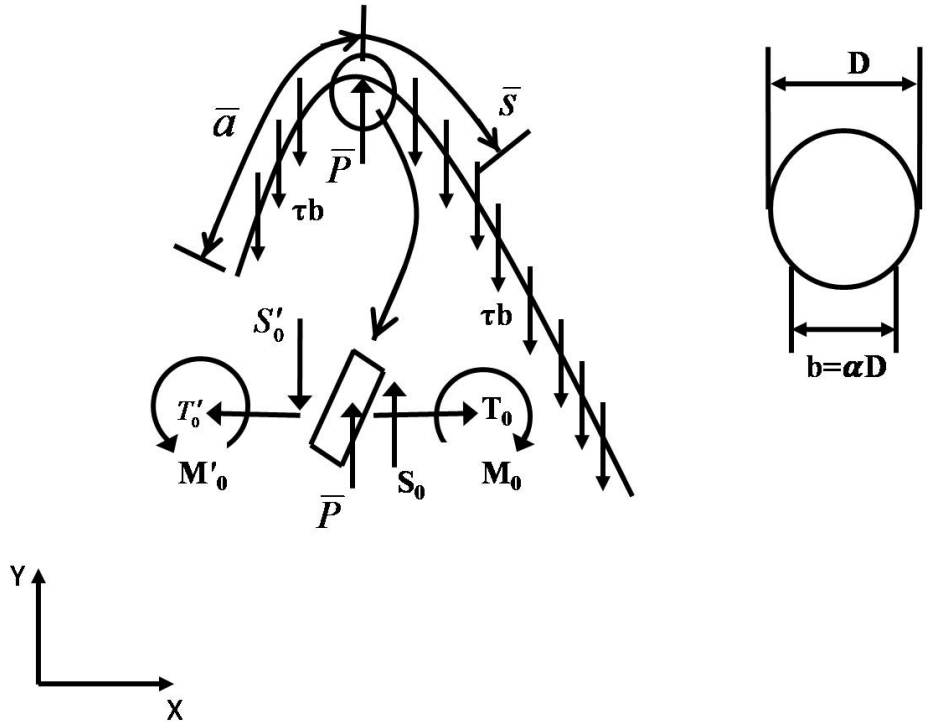

Figure 2. Schematic representation of non-symmetric loading of a CNT.

Non-Symmetric Loading

In this case the CNT is dragged along the substrate by applying the force away from the midpoint. A schematic of this case is shown in Figure 2. By writing the equations for the non-symmetric case from the general equation (1), we obtain

$$EI\frac{d^2\psi}{d\bar{s}^2} + \frac{\bar{P}}{L}(L - \bar{a} - \bar{s})\cos\psi = 0,\ 0 < \bar{s} < L - \bar{a} \tag{4}$$

$$EI\frac{d^2\psi}{d\bar{s}^2} - \frac{\bar{P}}{L}(\bar{a} + \bar{s})\cos\psi = 0, \qquad -\bar{a} < \bar{s} < 0 \tag{5}$$

Here $\bar{a}$ is the distance from the left end of the beam to where the load is applied. It will be shown that this non-symmetric case will give better resolution than the

symmetric condition case in determining the frictional interaction between the CNT and substrate. Here the boundary conditions are that the bending moments at both ends of the CNT are zero. However the angle ψ at the loading point may or may not vanish. Moreover the field equations (4)-(5) require continuity conditions at the load point. These conditions are that the angle of rotation and bending moment are each continuous at $\bar{s} = 0$, i.e.

$$\psi(0^-) = \psi(0^+), \quad \psi'(0^-) = \psi'(0^+) \tag{6}$$

Non-dimensional Analysis

In order to generalize the analysis for different lengths and diameters of CNTs, we convert the equations into dimensionless form. The dimensionless quantities are

$$P = \frac{\bar{P}L^2}{EI}, \quad s = \frac{\bar{s}}{L}, \quad a = \frac{\bar{a}}{L}, \quad \tau = \frac{\bar{\tau} b L^3}{EI} = P \tag{7}$$

Rewriting equations (2)-(6) gives

$$\frac{d^2\psi}{ds^2} + P(0.5 - s)\cos\psi = 0, \quad 0 < s < 1/2 \ , \ \psi(0) = 0 \ , \ \psi'(1/2) = 0 \tag{8}$$

$$\frac{d^2\psi}{ds^2} + P((1-a) - s)\cos\psi = 0, \quad 0 < s < (1-a), \quad \psi(0^-) = \psi(0^+), \ \psi'(1-a) = 0 \tag{9}$$

$$\frac{d^2\psi}{ds^2} - P(a + s)\cos\psi = 0, \quad -a < s < 0, \quad \psi'(0^-) = \psi'(0^+), \ \psi'(-a) = 0 \tag{10}$$

This dimensionless conversion allows a single result to be used for a variety of problems through a simple scaling.

Numerical Solution

The above equations are solved as initial value problems using standard numerical integration software along with a shooting method. Thus for the

symmetric case an initial guess is needed for the dimensionless moment $\psi'(0)$. Equation (8) is then integrated in order to determine $\psi'(1/2)$; the correct value of $\psi'(0)$ is the one which causes $\psi'(1/2)$ to equal zero. This condition corresponds to solving a single nonlinear algebraic equation. For the non-symmetric case, initial guesses for $\psi(0)$ and for $\psi'(0)$ are needed. Equations (9) and (10) were then each integrated in order to determine $\psi'(1\text{-}a)$ and $\psi'(-a)$. The correct values of $\psi(0)$ and $\psi'(0)$ are found by solving the nonlinear equations corresponding to $\psi'(1\text{-}a)=0$ and $\psi'(-a)=0$.

As a result of this numerical solution procedure the angle ψ is determined at all points along the CNT. The final deformed shape of the CNT is then determined from

$$X(s) = \int_0^s \cos(\psi) ds$$

$$Y(s) = -\int_0^s \sin(\psi) ds \tag{11}$$

using numerical integration. By observing the deformed shape, it is then possible to calculate the frictional interaction which occurred during sliding.

RESULTS AND DISCUSSION

Symmetric Loading

Results were obtained for symmetric loading using the method outlined in the previous section. Figure 3 shows the variation of rotation angle (ψ) at various points on the CNT as a function of the dimensionless shear stress (τ) and also of the dimensioned frictional shear stress ($\bar{\tau}$). In Figure 3, and in subsequent figures, $\bar{\tau}$ is computed from τ using typical values of E = 1 TPa, D = 1.3 nm, and L = 300 nm. Note from Figure 3 that as the position away from the midpoint increases, so does the angle of rotation. The maximum angle of rotation that can be achieved is 90°. Also as the value of the shear stress (or equivalently the load) increases, so does the rotation angle. However, as the shear stress

increases, the sensitivity of the angle of rotation to the frictional shear stress decreases.

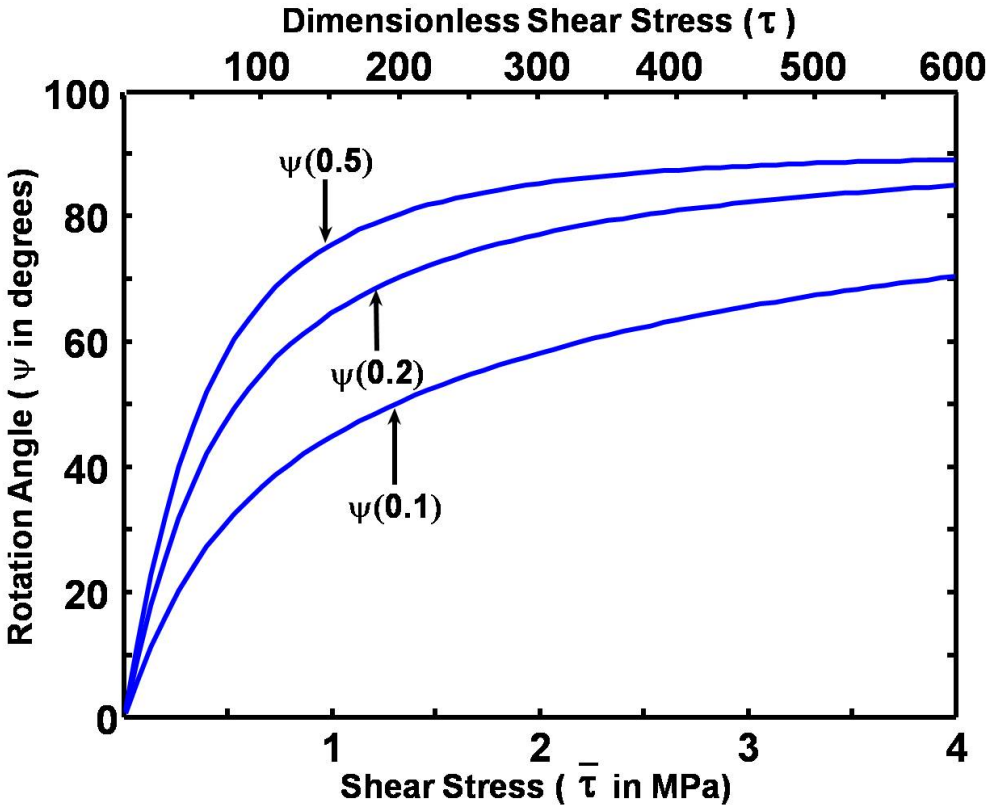

Figure 3. Rotation angle (ψ) vs. shear stress ($\bar{\tau}$) and vs. dimensionless shear stress (τ).

The dimensionless moment ψ' is equal to the reciprocal of the dimensionless radius of curvature. A plot of the dimensioned radius of curvature at the load point vs. either shear stress or dimensionless load is shown in Figure 4.

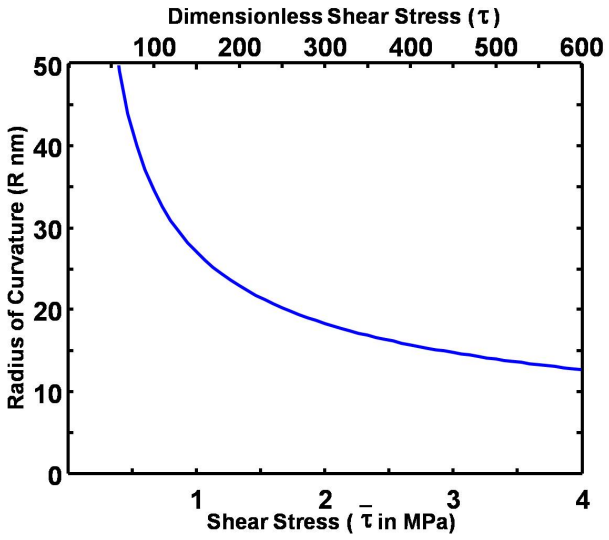

Figure 4. Variation of radius of curvature (*r*) at the load point with shear stress ($\bar{\tau}$) and with dimensionless shear stress (τ).

As indicated in [15], the minimum radius of curvature for a single-walled CNT to be in the elastic range is about 8 nm. Here the smallest value of *R* is approximately 12 nm which confirms that the simulation was carried out in the elastic range. It is noted that the assumption of a point load implies that the radius of curvature of the AFM tip is less than the radius of curvature of the deformed CNT. Thus the results shown in Figure 4 also allow the checking of this assumption for a particular set of results. Note that a commercially available AFM tip can have a radius of curvature as low as 10 nm.

As discussed earlier, by knowing the rotation angle at every coordinate along the CNT and using numerical integration methods, we can determine the final deformed shape of CNT. A plot of such deformed shapes for various values of dimensionless load is shown in Figure 5. As stated earlier an increase in frictional shear stress leads to an increase in the bending of the CNT. In order for this measurement method to be practical there needs to be sufficient sensitivity of the shape to the shear stress interaction. It is seen that for τ greater than about 300 (which corresponds to *L/D* = 230 for the typical dimensioned case considered with $\bar{\tau} = 2\,\mathrm{MPa}$**),** reduced sensitivity becomes an issue. Note that this maximum aspect ratio varies weakly (as the one-third power) with the shear stress. Similarly for low values of τ the CNT may not bend sufficiently (i.e. for τ

less than about 25 from Figure 3, which for the typical case corresponds to *L/D* = 100) and hence may then move in a combination of rolling and sliding motion.

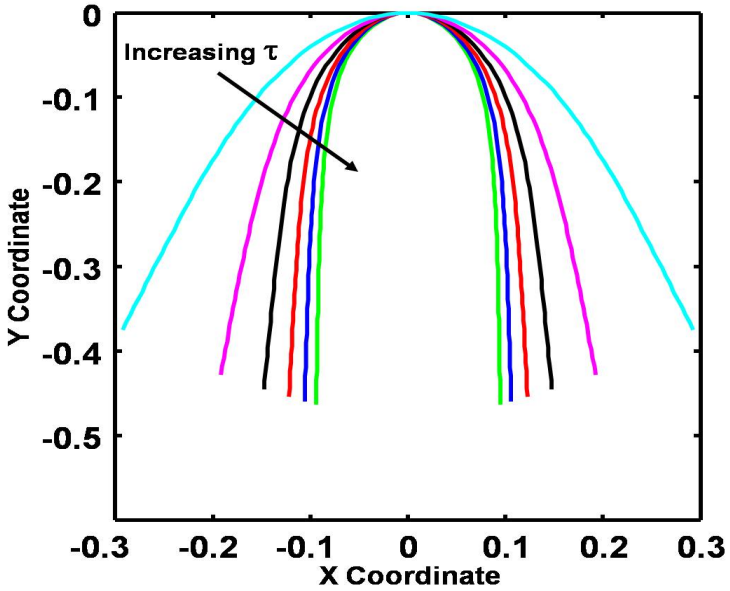

Figure 5. Final shape of cnt in symmetric loading for various values of τ (100, 200, 300, 400, 500, 600).

Non-Symmetric Loading

Results were also obtained for the non-symmetric case using the method outlined in the previous section. However in this case there is the possibility of different equilibrium positions existing. One equilibrium position is for the CNT to remain straight and oriented in the same direction as the force; the other equilibrium is that the tube bends. Let τ_c be the critical shear stress for the change of equilibrium positions. Then if $\tau > \tau_c$, the final shape of the CNT is bent and if $\tau < \tau_c$ the final shape of the CNT is straight. This behavior is analogous to buckling of a bar under a distributed load. The critical load τ_c is also a function of the load point location (*a*). If the point of application of the load is very close to the end of the CNT, shear stress will not cause the CNT to bend. However in such a configuration it is likely that the CNT will slide off the AFM tip rather than adhere to it as the AFM tip moves along the substrate. On the other hand if the point of application of the load is close to the midpoint it is more likely that the

CNT will bend. It is noted that in solving the symmetric problem, the rotation angle at the load point was forced to be zero which precluded the existence of multiple equilibrium positions.

The simulations were carried out for different values of 'a' varying from 0.3–0.5. Figure 6 shows the variation of rotation angle $\psi(0)$ with the dimensionless shear stress (τ) and with the shear stress $\bar{\tau}$. Different curves correspond to different values of the load point (a).

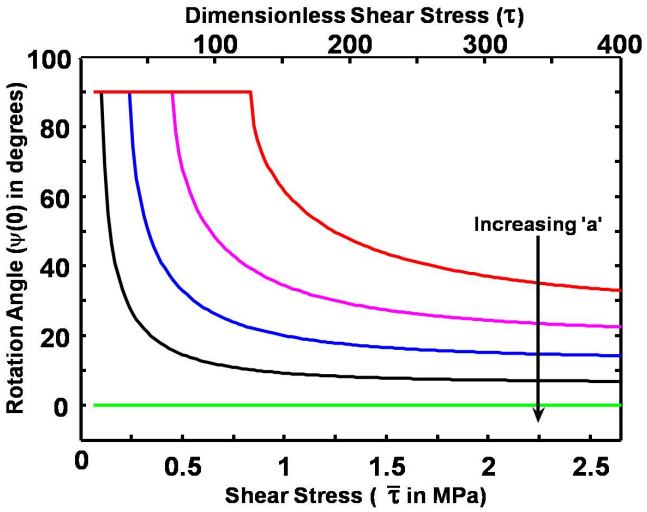

Figure 6. Variation of rotation angle $\psi(0)$ with shear stress ($\bar{\tau}$) and with dimensionless shear stress (τ) for non-symmetric condition for various values of 'a' (0.3, 0.35, 0.4, 0.45, 0.5).

For sufficiently small values of the shear stress each of the curves start with $\psi(0) = 90^0$, i.e. the straight configuration. As the load moves further away from the midpoint, the shear stress required to produce a bent configuration increases. The sensitivity of $\psi(0)$ with shear stress becomes low as τ continues to increase.

Figure 7 shows the variation of dimensionless moment (from which the radius of curvature can be readily determined) at the loading point with respect to the shear stress for various values of 'a'. The curvature increases with increasing shear stress and/or increasing load point distance (a).

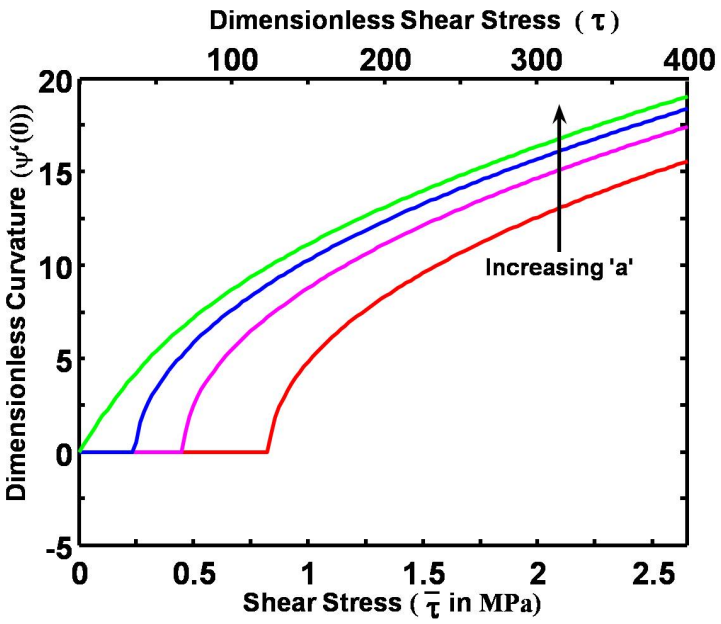

Figure 7. Variation of ψ′(0) with shear stress ($\bar{\tau}$) and with dimensionless shear stress (τ) for various values of 'a' (0.3, 0.35, 0.4, 0.5).

Figure 8 shows the variation of the rotation angle at the right (long) end of the CNT with respect to the shear stress for various values of load point location (*a*). As the shear stress increases, this end of the CNT rotates through an angle which tends to 90^{o}. For $a = 0.3$, the CNT remains straight until $\tau \cong 125$ at which point it bends, but the rotation of the longer end still remains close to 90^{0}. When the point of application of the load is closer to the midpoint there is a greater variation of this rotation angle with an increase in shear stress. Figure 9 shows the variation of angle at the left (short) end of beam with respect to shear stress for a variety of load point locations. Here there is a transition from positive to negative angles as the load decreases. It is noted that for values of τ as high as 400 (corresponding to an aspect ratio of about 250) there is still sufficient sensitivity of the rotation angle to the shear stress.

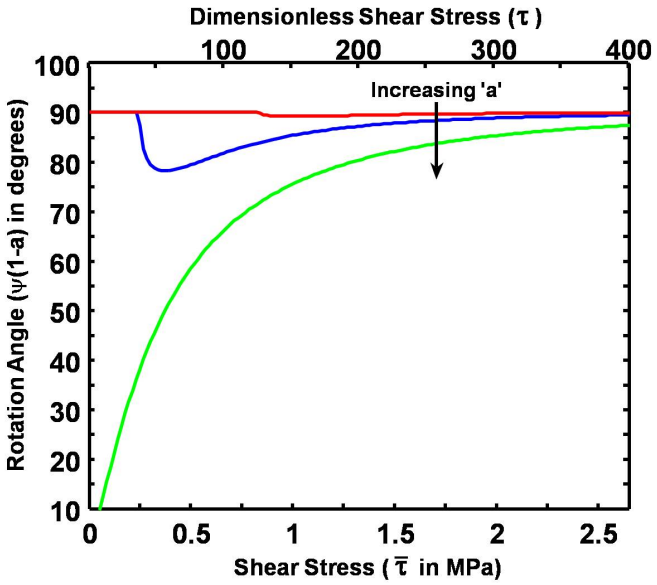

Figure 8. Rotation angle ψ(1-a) (right end of beam) vs. shear stress ($\bar{\tau}$) and vs. dimensionless shear stress (τ) for various values of 'a' (0.3, 0.4, 0.5).

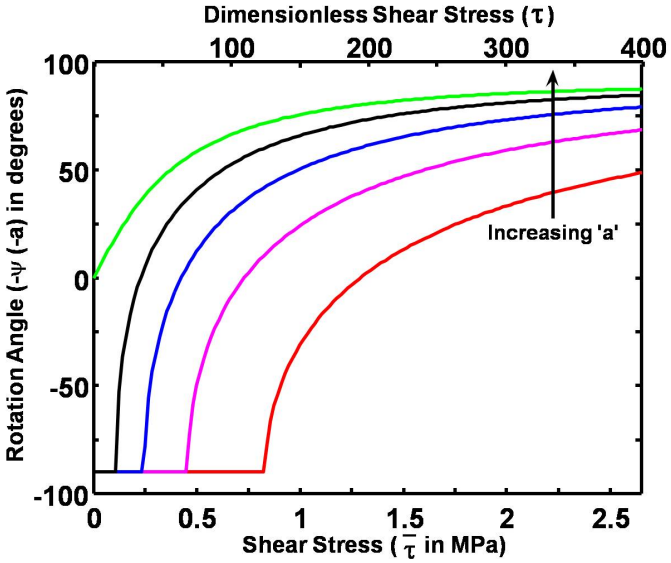

Figure 9. Variation of rotation angle (ψ (-a)) with shear stress ($\bar{\tau}$) and with dimensionless shear stress (τ) for various values of 'a' (0.3, 0.35, 0.4, 0.45, 0.5).

Figures 10 and 11 show the final shape of the CNT for a = 0.4 and a = 0.3 respectively. The two different equilibrium positions can be seen in Figure 11 for a = 0.3. Smaller friction leads to a straight tube in the direction of travel while larger friction produces a bent tube. A straight tube equilibrium does not occur for a = 0.4 in the range investigated, although such solutions exist for smaller values of τ as indicated in Figures 8 and 9. As was mentioned the resolution to determine the frictional interaction is greater for the case of non-symmetric loading than for symmetric loading. Beyond a certain load the change in shape with increasing frictional interaction becomes insufficient to obtain reasonable resolution. However, as stated earlier, if the value of "a" is too small, the tube can slip off of the AFM tip.

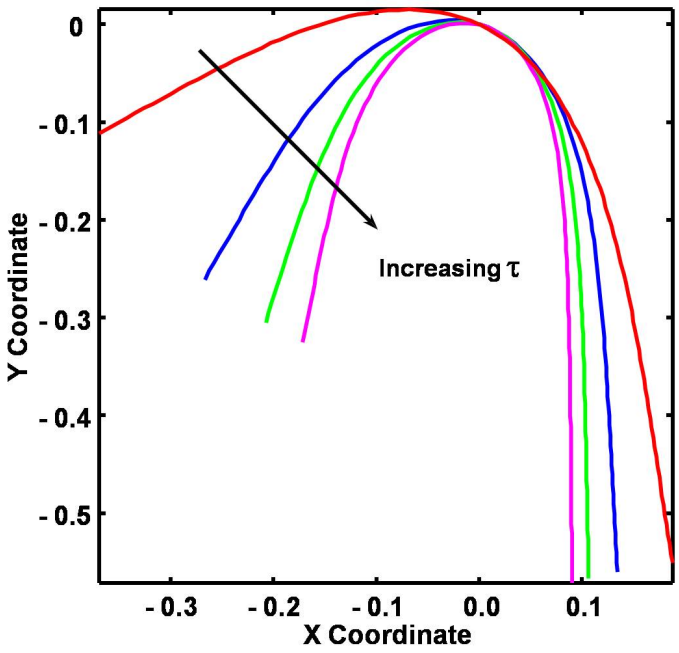

Figure 10. Deformed shape of nanotube for a = 0.4 and for various values of shear stress τ (100, 200, 300, 400).

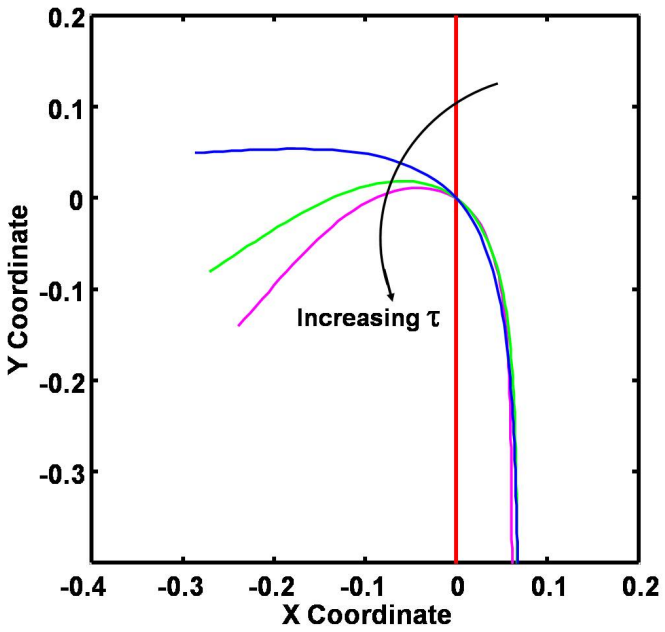

Figure 11. Final shape of nanotube for a = 0.3 and for various values of shear stress τ (100, 200, 300, 400).

Dragging of CNT on an Anisotropic Substrate

Modeling of an Anisotropic Substrate:

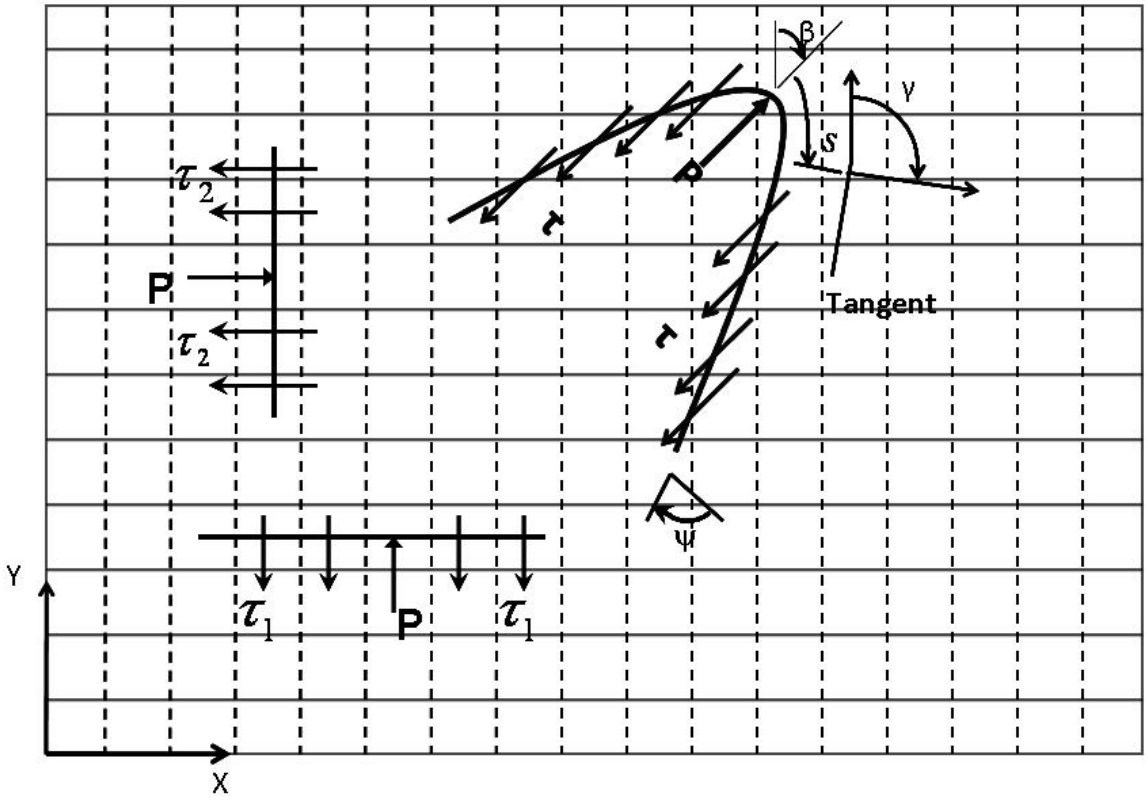

Figure 12: CNT placed on an anisotropic substrate

The above figure shows a simplified model of a nanotube on an anisotropic substrate. Substrate is represented by dotted lines along the vertical direction and continuous lines in horizontal direction stating that there are two independent directions and material properties differ along these two directions.

When the nanotube is placed parallel to the horizontal direction the shear stress offered by the substrate is designated as τ_1. On the other hand when nanotube is placed along the vertical direction shear stress offered by the substrate is designated as τ_2.Now if the nanotube is placed along an inclined axis at an angle to both the cases specified above , the shear stress offered by the substrate is taken to be τ. This shear stress 'τ' should be a function of τ_1, τ_2 and the angle of inclination.

As specified earlier angle 'ψ' is the angle between the tangent at any coordinate of the CNT and an axis perpendicular to the loading direction. Because of the direction dependent shear stress an angle of 'β' is included in the analysis which is taken as the angle between the loading direction and the y-axis. The direction between the line perpendicular to the tangent at a point and the y-axis is taken to be angle 'γ'. By geometry this angle is an addition of β and ψ. 'τ' is now a function of τ_1, τ_2 and γ and expressed as

$$\tau = \frac{\tau_1 + \tau_2}{2} + \frac{\tau_1 - \tau_2}{2}\cos(2\gamma) \qquad \gamma = \psi + \beta \tag{12}$$

Analysis of Anisotropic Substrate:

The deformation still follows elastica theory as in first case. Based on the general equation (1) equations for the particular case can be formed.

$$EI\frac{d^2\psi}{d\bar{s}^2} - (\bar{S}_0 + \bar{\tau}b\bar{s})\cos\psi = 0 \qquad 0 < \bar{s} < L - \bar{a} \tag{13}$$

$$EI\frac{d^2\psi}{d\bar{s}^2} - (\bar{S}_0^{'} + \bar{\tau}b\bar{s})\cos\psi = 0 \qquad -\bar{a} < \bar{s} < 0 \tag{14}$$

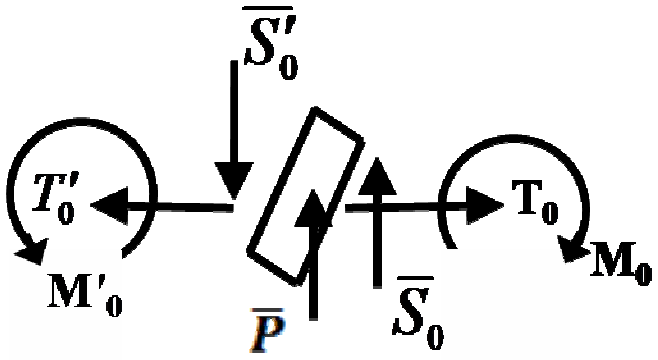

Figure 13: Shear Force at the loading point

By equilibrium

$$\overline{S}_0 = -\int_0^{L-\overline{a}} \overline{\tau} b d\overline{s} \tag{15}$$

$$\overline{S}'_0 = \int_{-\overline{a}}^{0} \overline{\tau} b d\overline{s}$$

The above equations are the shear force for right hand side and left hand side beam respectively. A schematic of shear force diagram is shown in figure 13. For a symmetric case since the load is applied at the midpoint, the tangent to the CNT at that point is in the x-direction. Hence one of the boundary conditions is zero rotation at the point of application of the load. The second boundary condition is that the bending moment at the free end of the CNT is zero. These conditions are written as

$$\psi(0) = 0 \qquad EI\psi'(L/2) = 0 \tag{16}$$

For a non-symmetric case '$\overline{a}$ ' is the distance from the left end of the beam to where the load is applied. Here the boundary conditions are that the bending moments at both ends of the CNT are zero. However the angle ψ at the loading point may or may not vanish. Moreover the field equations require continuity conditions at the load point. These conditions are that the angle of rotation and bending moment are each continuous at $\overline{s} = 0$, i.e.

$$\psi(0^-) = \psi(0^+)\ ,\ \psi'(0^-) = \psi'(0^+)\ ,\ \psi'(L-\overline{a}) = 0\ ,\ \psi'(-\overline{a}) = 0 \tag{17}$$

following the same rules of generalization equations are converted into dimensionless forms

$$s = \frac{\overline{s}}{L}\ ,\ a = \frac{\overline{a}}{L}\ ,\ \tau = \frac{\overline{\tau} b L^3}{EI}\ ,\ S_0 = \frac{\overline{S}_o L^2}{EI},\ S'_0 = \frac{\overline{S}'_o L^2}{EI} \tag{18}$$

Rewriting equations

$$\frac{d^2\psi}{ds^2} - (S_0 + \tau s)\cos\psi = 0, \qquad 0 < s < (1-a)$$

$$\psi(0^-) = \psi(0^+), \quad \psi'(1-a) = 0 \tag{19}$$

$$\frac{d^2\psi}{ds^2} - (S_0' + \tau s)\cos\psi = 0, \qquad -a < s < 0$$

$$\psi'(0^-) = \psi'(0^+), \quad \psi'(-a) = 0 \tag{20}$$

$$S_0 = -\int_0^{1-a} \tau ds$$

$$S_0' = \int_{-a}^{0} \tau ds \tag{21}$$

Numerical Solutions:

The above equations are solved as initial value problems using standard numerical integration software along with a shooting method. Thus for a case an initial guess is needed for the angle at the loading point Ψ(0) ,dimensionless moment $\psi'(0)$ and an initial guess for the shear force (S_0 and S_0') on both sides of the beam . Equation is then integrated in order to determine ψ'(1-a) and $\psi'(-a)$.The correct value is the one which causes ψ' at both ends to equal zero . Because of orientation dependent shear stress the shear force on either side of beam is not constant and it is found by integrating the shear stress expression over the length. So for the given initial guess apart from converging for moment at either end to be zero care should be taken to see that the shear force equation is also satisfied. The condition of convergence is taken approximately equal to zero since it is a numerical solution. The approximation is made only after the sixth decimal place that is 1e-6 is approximately equal to zero.

As a result of this numerical solution procedure the angle ψ is determined at all points along the CNT. The final deformed shape of the CNT is then determined from

$$X(s) = \int_0^s \cos(\psi) ds$$

$$Y(s) = -\int_0^s \sin(\psi) ds \qquad (22)$$

Results and Discussion:

The analysis was carried out two different ways. First part includes the effect of angle β on a consistently increasing τ_2/τ_1 ratio for different values of length 'a'. For this the term $\tau_{ave} = (\tau_1 + \tau_2)/2$ is maintained constant and the ratio of τ_2/τ_1 is varied.

Symmetric loading:

Figure 14 shows the variation of rotational angle Ψ(0) with respect to τ_2/τ_1 ratio. Here the graph is plotted for a constant value of a= 0.5 and $\tau_{ave} = 300$ .The value of angle of inclination is varied to find the result. For the extreme cases of angle β (0^0 and 90^0) system is symmetric and hence the rotational angle is zero. For other values of β there is an increase in the rotation angle with increasing τ_2/τ_1 ratio. The rotation angle does not vanish here because of the asymmetry caused by the angle of inclination.

Figure 15 shows the variation of dimensionless moment ψ' as a function of τ_2/τ_1. Dimensionless moment is equal to the reciprocal of the dimensionless radius of curvature. Hence ψ' increases with increasing ratio of shear stress for smaller values of β. When β approaches 90^0 ψ' decreases with increase in shear stress. For $\tau_2/\tau_1 < 1$ there is an increase in the dimensionless moment with increasing β stating that shear stress offered by the substrate is more. On the other hand for $\tau_2/\tau_1 > 1$ the dimensionless moment decreases with increasing β stating that shear stress offered by the substrate is less in turn less friction is offered . The value of dimensionless moment for extreme cases of τ_2/τ_1 is equal in magnitude. This is because for the extreme cases value of shear stress are interchanged and hence the values are same.

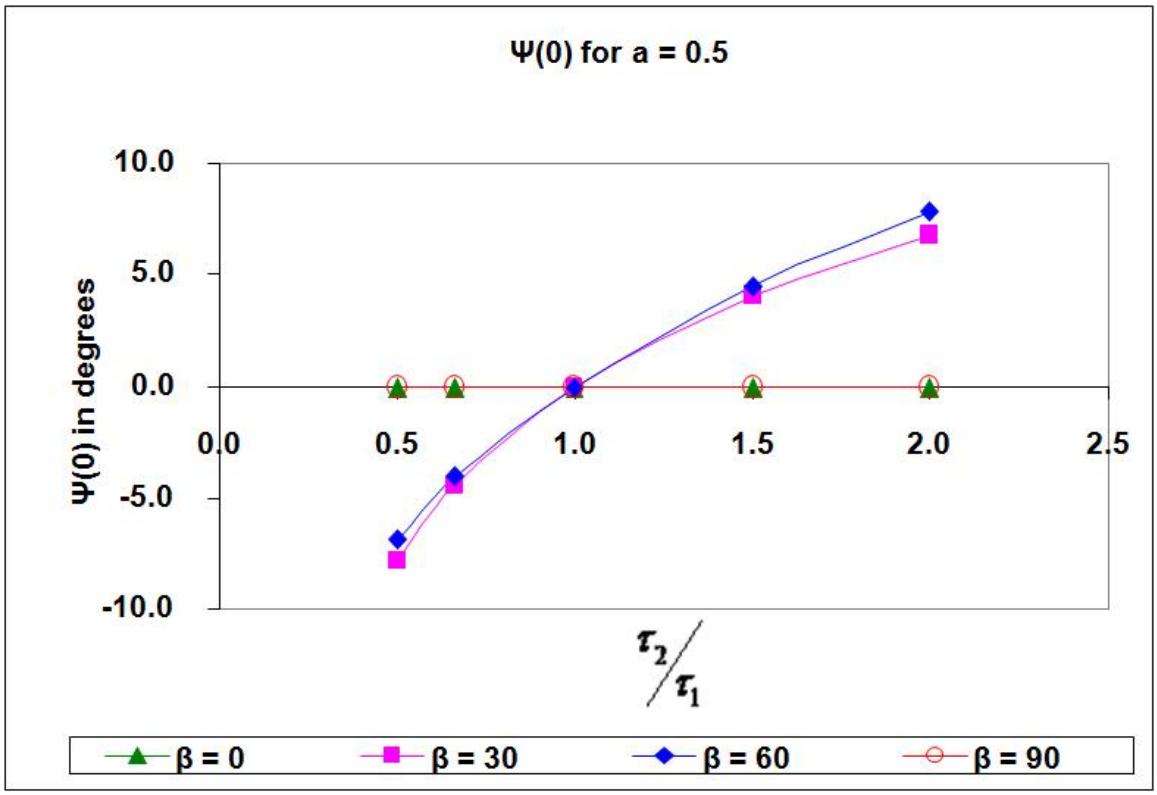

Figure 14: Plot showing the variation of Ψ(0) for a = 0.5 and $\tau_{ave} = 300$

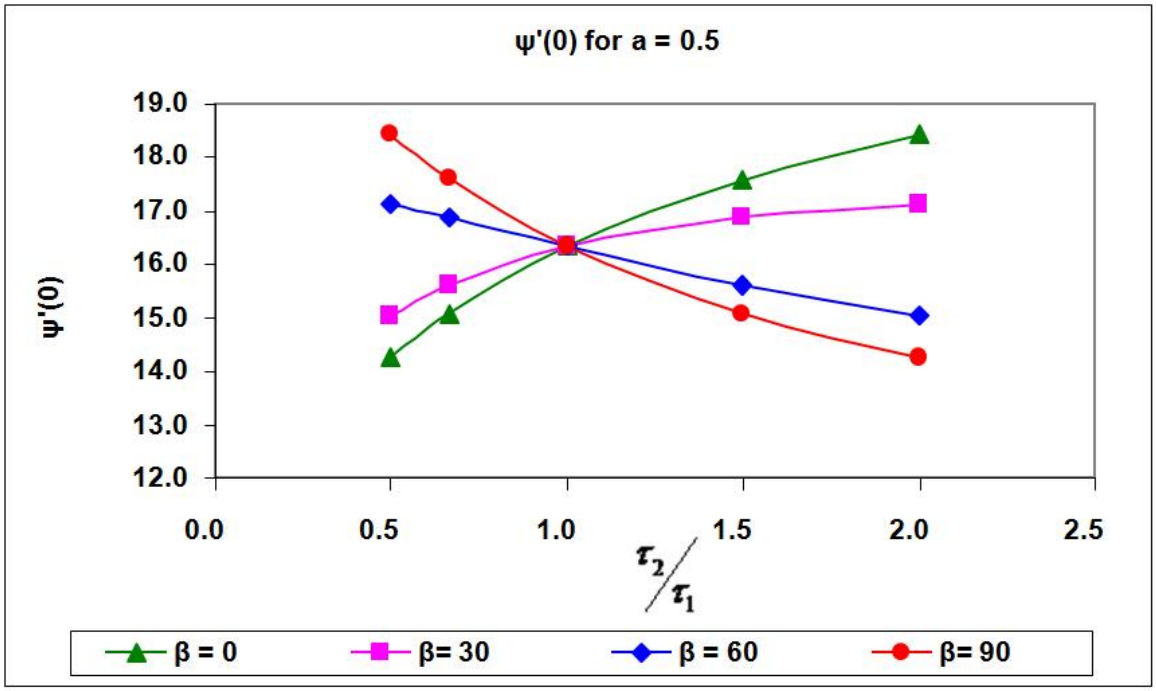

Figure 15: Plot showing the variation of Ψ'(0) for a = 0.5 and $\tau_{ave} = 300$

For a given value of β in the 0-90^0 degree range the value of Ψ(1-a) increases with increasing τ_2/τ_1 ratio except for the extreme cases of β. The angles are equal for the extreme cases because the nanotube is subjected to a symmetric condition. If the amount of shear stress decreases for the same value of applied load there will be more bending of nanotube and hence more angle of rotation. On the other hand for β = 30^0 and 60^0 angle of rotation at the left end of beam -Ψ(-a) decreases with increasing τ_2/τ_1 . Figures 16 and 17 show the variation of rotation angle to an increasing τ_2/τ_1 ratio.

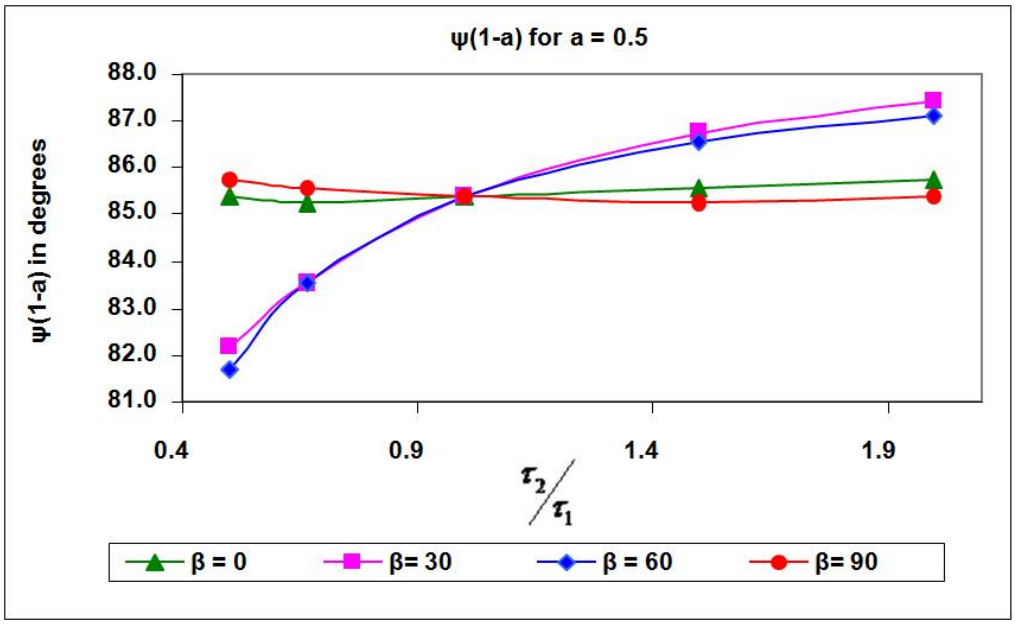

Figure 16: Plot showing the variation of ψ(1-a) for a = 0.5 and $\tau_{ave} = 300$

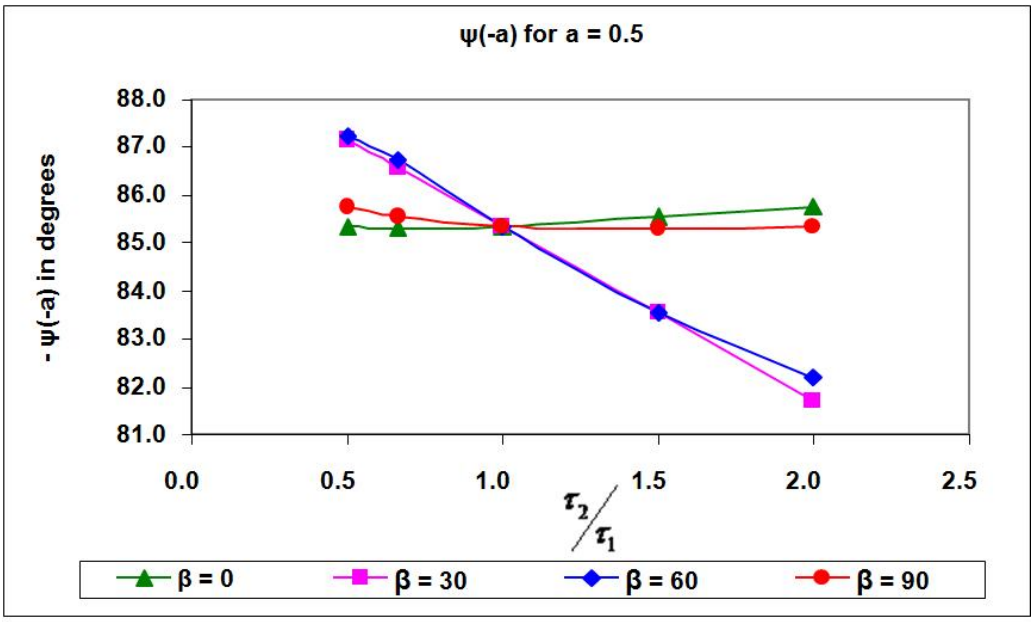

Figure 17: Plot showing the variation of ψ(-a) for a = 0.5 and $\tau_{ave} = 300$

By knowing the rotation angle at every coordinate along the CNT and using numerical integration methods final deformed shape of the nanotube can be determined.The final shape of the nanotube for a constant value of β and varying τ_2/τ_1 is shown in Figures 18, 19, 20 and 21. The deformed shape of the nanotubes is plotted for a constant value of $\tau_{ave} = 300$.

In the case of increasing β the shear stress offered by the substrate is more when $\tau_2/\tau_1 < 1$. The amount of bending of the nanotube is proportional to the radius of curvature which is determined from the dimensionless moment. For the same value of load final shape of nanotube is plotted for varying shear stress ratio τ_2/τ_1. The shear stress ratio is changed by changing the substrate. When the nanotube is placed horizontal effect of shear stress τ_1 is more as compared to τ_2. For higher value of τ_1 there is more shear stress offered by the substrate for the applied load and hence less bending. When the value of shear stress τ_1 decreases for the same value of applied load there is more bending of nanotube.

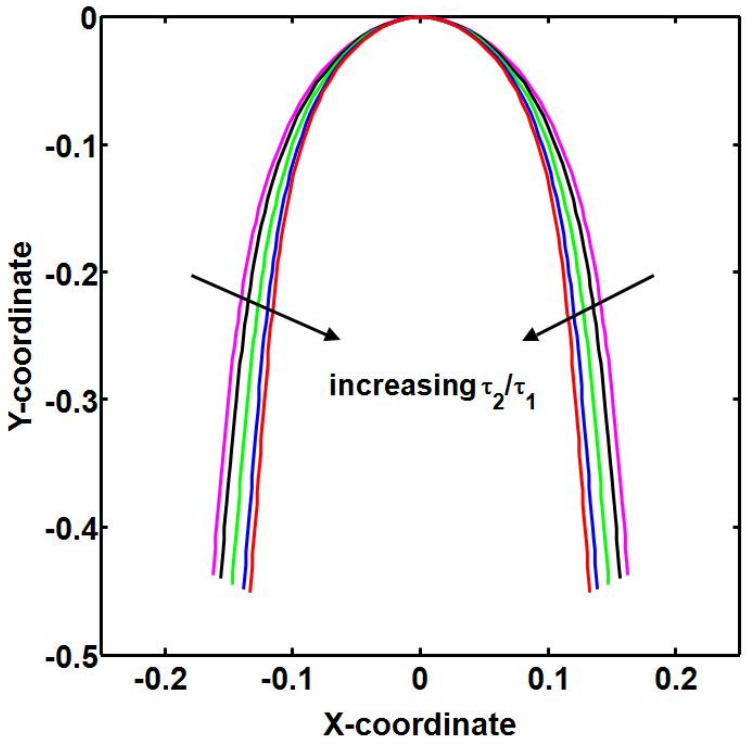

Figure 18: Final shape of nanotube for a = 0.5 and β = 0(τ_{ave} = 300 and τ_2/τ_1 = 0.5, 0.67 ,1, 1.5, 2)

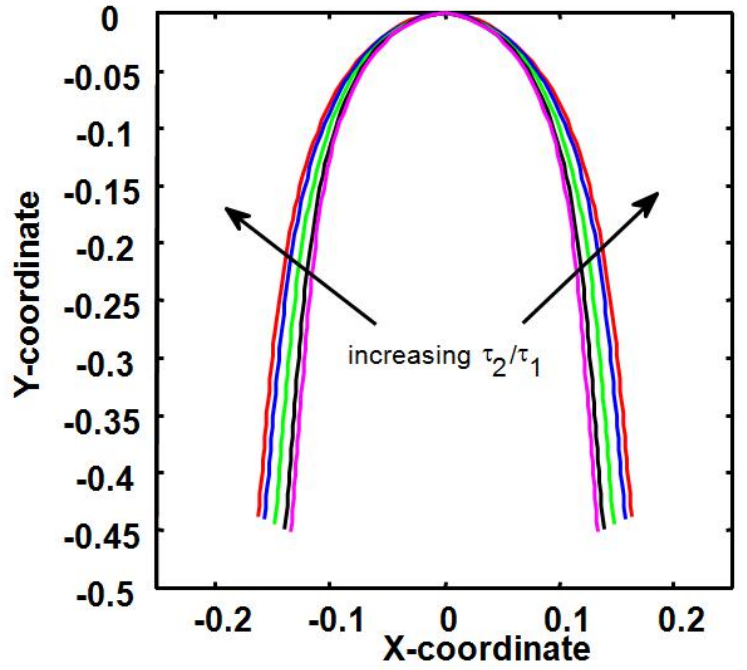

Figure 19: Final shape of nanotube for a = 0.5 and β = 90 (τ_{ave} = 300 and τ_2/τ_1 = 0.5, 0.67 ,1, 1.5, 2)

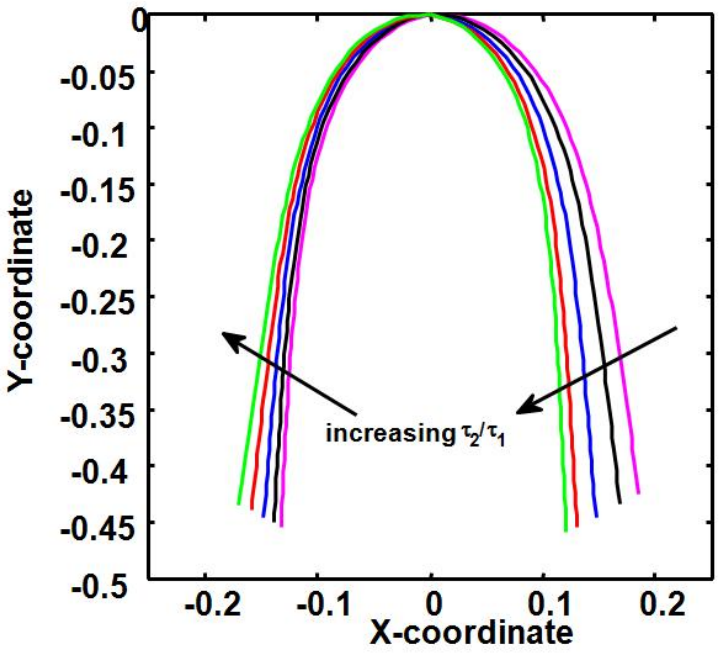

Figure 20: Final shape of nanotube for a = 0.5 and β = 30(τ_{ave} = 300 and τ_2/τ_1 = 0.5, 0.67 ,1, 1.5, 2)

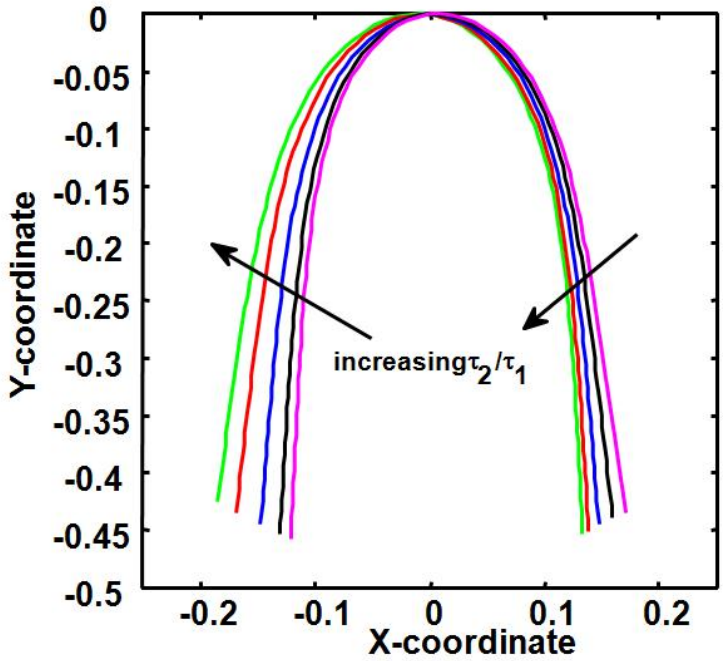

Figure 21: Final shape of nanotube for a = 0.5 and β = 60 (τ_{ave} = 300 and τ_2/τ_1 = 0.5, 0.67 ,1, 1.5, 2)

When the nanotube is placed vertical effect of shear stress τ_2 is more as compared to τ_1. For higher value of τ_2 there is more shear stress offered by the substrate for the applied load and hence less bending. When the value of shear stress τ_2 decreases for the same value of applied load there is more bending of nanotube.

For the inbetween cases of angle of orientation β (30^0,60^0) the effect of shear stress τ_1 is more for the right side beam and left side beam is affected by shear stress τ_2.

Varying Shear Stress Average:

The above analysis is carried out for a constant value of τ_{ave} = 300. Now if the system is subjected to varying average shear stress the following results can be achieved. The only disadvantage with this analysis is that the initial guesses of angle of rotation, moment and the shear forces on either side of the beam needs to be a nominal guess for the problem to converge. So the analysis is carried out for a series of τ_{ave} ranging from 300-100 which holds good for all cases discussed below. Variation of the angle of rotation at the loading point as well as at either ends of the CNT and moment for individual cases are shown below. Here apart from varying the shear stress (τ_{ave}) ratio τ_2/τ_1 is also varied.

Figures 23(a) and 24(a) shows the variation of angle of rotation with respect to τ_{ave}. The analysis is carried out for various values of applied load and for various substrates in terms of ratio of shear stress. The angle of rotation at the loading point increases with increasing τ_{ave} for substrates having higher values of shear stress τ_1. The results are reversed for substrates having higher value of shear stress τ_2. The value of angle of rotation for the symmetric cases of β=0^0 and β=90^0 are equal to zero. The value of angle of rotation decreases for a constant value of τ_2/τ_1 and increasing β.

Figure 22 (a), 23(b), 24(b) and 25(a) show the variation of dimensionless moment with respect to τ_{ave}. For τ_2/τ_1 <1 dimensionless moment increases with increasing τ_{ave} and vice versa for τ_2/τ_1 >1. As the value of shear stress τ_1 decreases the amount of bending of nanotube increases as less shear stress is

offered for the applied load. This states an increase in the bending moment at the loading point. On the other hand for $\tau_2/\tau_1 > 1$ dimensionless moment depends mainly on the shear stress τ_2.

Figure 22, 23, 24 and 25 show the variation of angle of rotation at either ends with respect to τ_{ave}. More the angle of rotation more is the bending of CNT. One can see that the value of angle of rotation for cases of $\beta=0^0$ and $\beta=90^0$ are exactly equal in magnitude which once again states that these are symmetric conditions. The sensitivity of the simulation to find the angle of rotation reduces for higher values of shear stress. For the same value of load if the shear stress offered by the substrate increases the amount of bending of nanotube decreases and so does the angle of rotation.

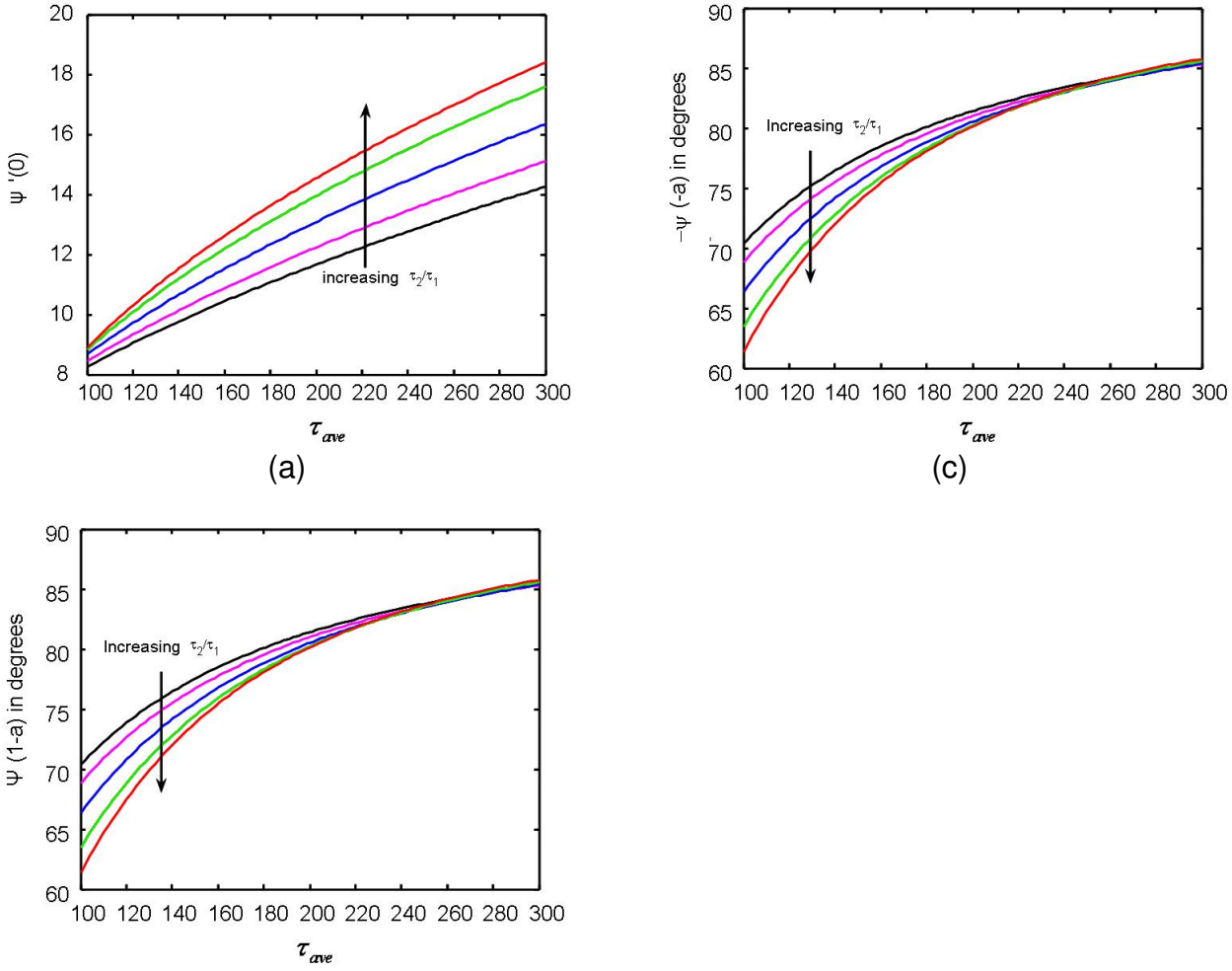

Figure 22: Plot showing the variation of (a) ψ'(0) , (b) ψ(1-a) and (c) Ψ(-a) vs. a series of τ_{ave} for a constant value of a = 0.5 and β=0.

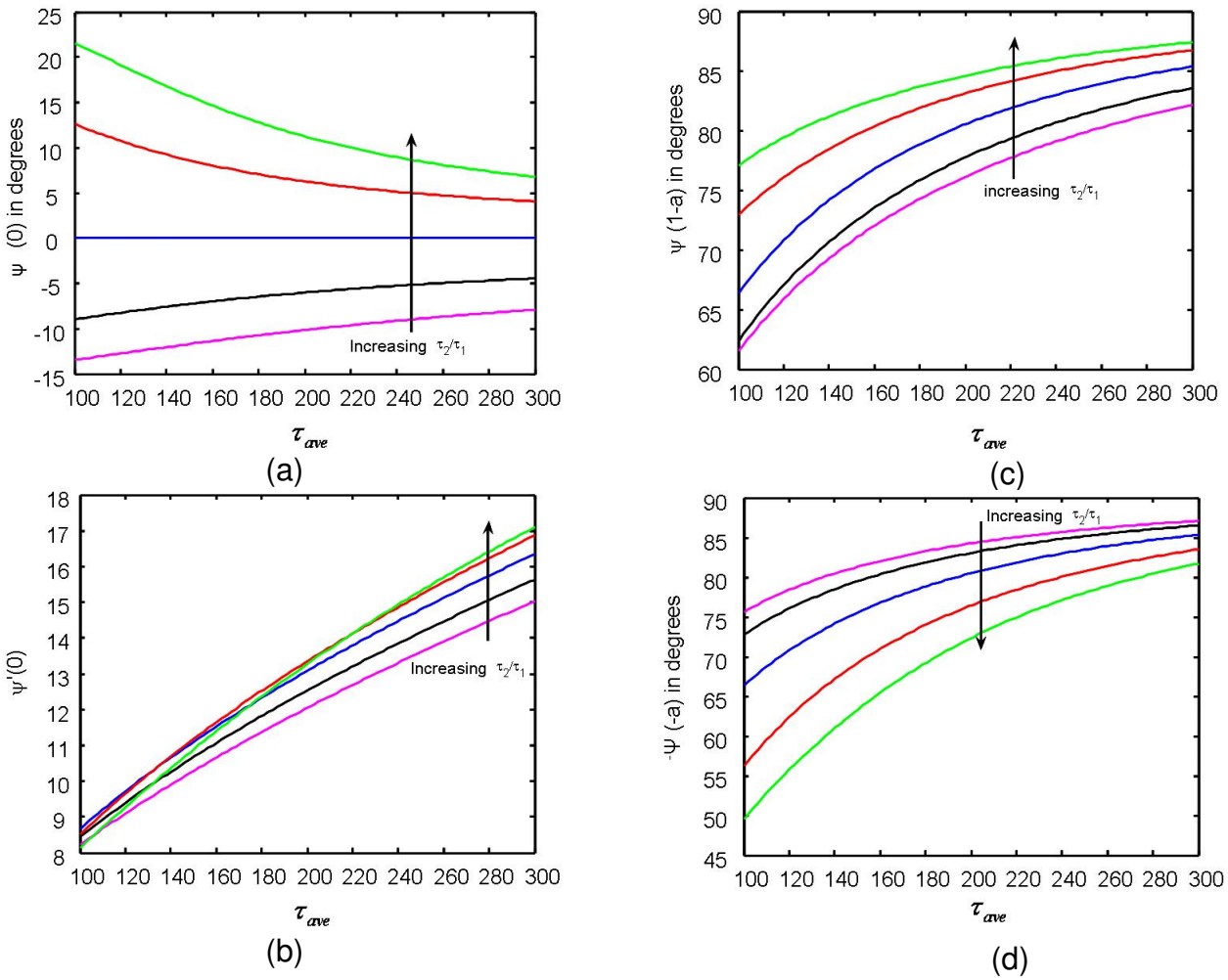

Figure 23: Plot showing the variation of (a) ψ (0), (b) ψ'(0) , (c) ψ(1-a) and (d) Ψ(-a) vs. a series of τ_{ave} for a constant value of a = 0.5 and β=30.

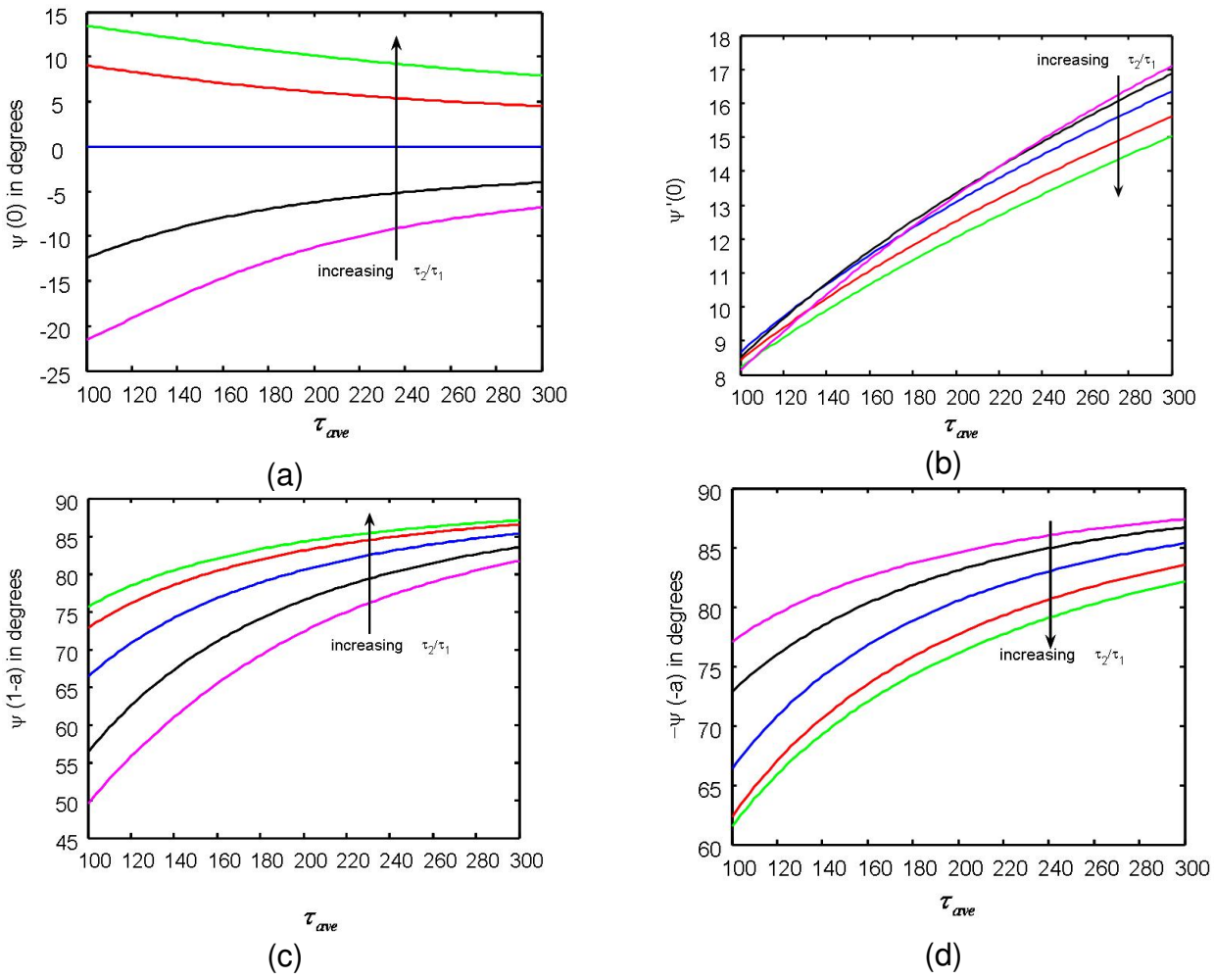

Figure 24: Plot showing the variation of (a) ψ (0), (b) ψ'(0) , (c) ψ(1-a) and (d) Ψ(-a) vs. a series of τ_{ave} for a constant value of a = 0.5 and β=60.

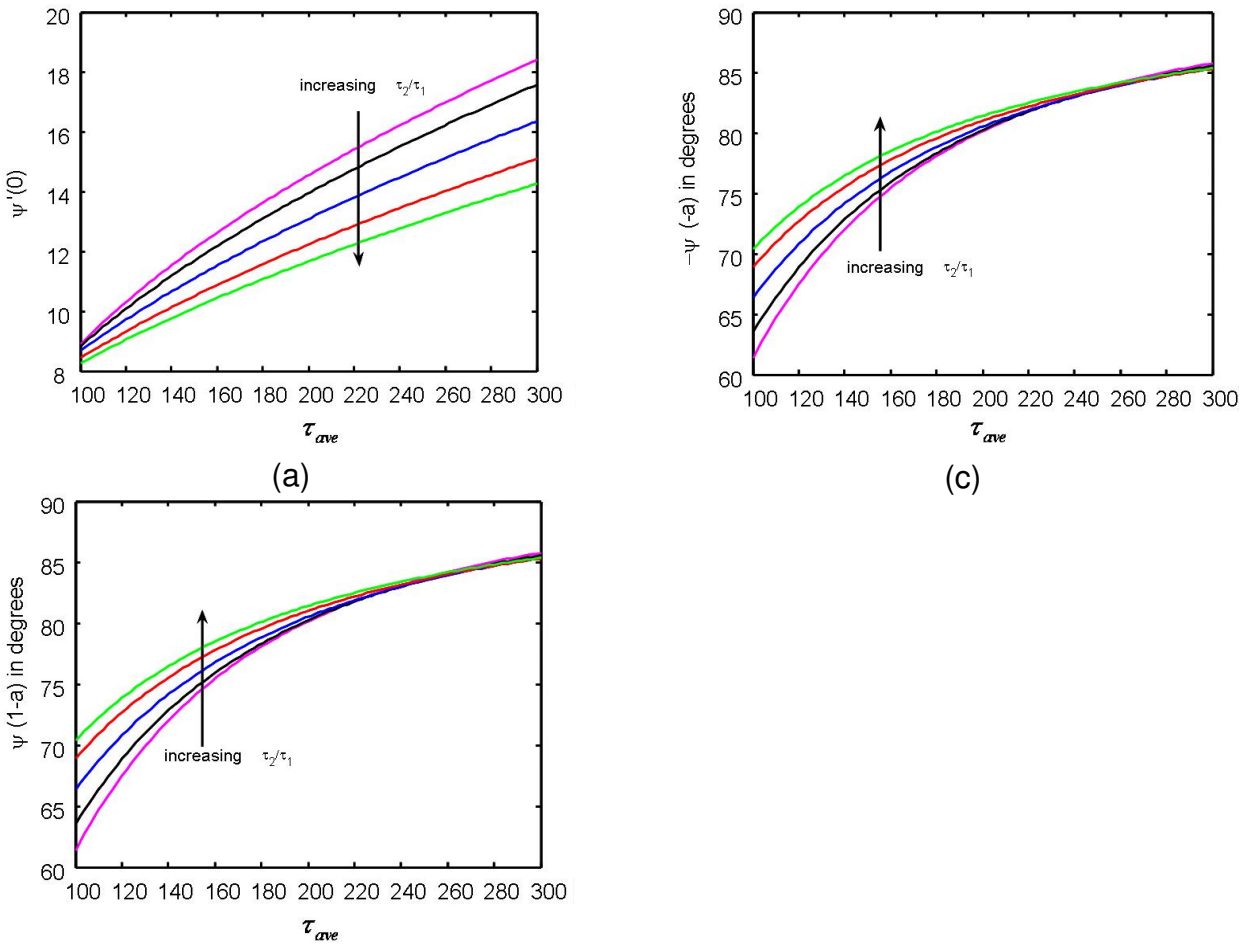

Figure 25: Plot showing the variation of (a) ψ'(0) , (b) ψ(1-a) and (c) Ψ(-a) vs. a series of τ_{ave} for a constant value of a = 0.5 and β=0

Non-Symmetric Loading:

In the following result section length 'a' is kept constant and angle β is varied. Figure 26 and 27 shows the variation of angle of rotation for varying τ_2/τ_1. Angle of rotation at the loading point increases with increasing τ_2/τ_1 for all cases of β except for the case of β = 90 where there is a decrease in the angle of rotation. The change in angle of rotation depends on shear stress offered by the substrate and also the effect of shear stress based on the orientation of the nanotube.

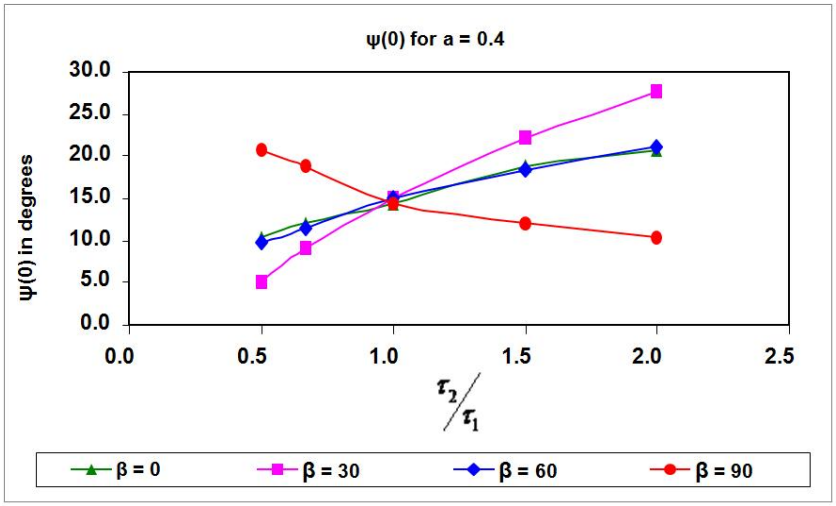

Figure 26: Plot showing the variation of ψ(0) for a = 0.4 (τ_{ave} = 300 and τ_2/τ_1 = 0.5, 0.67 ,1, 1.5, 2)

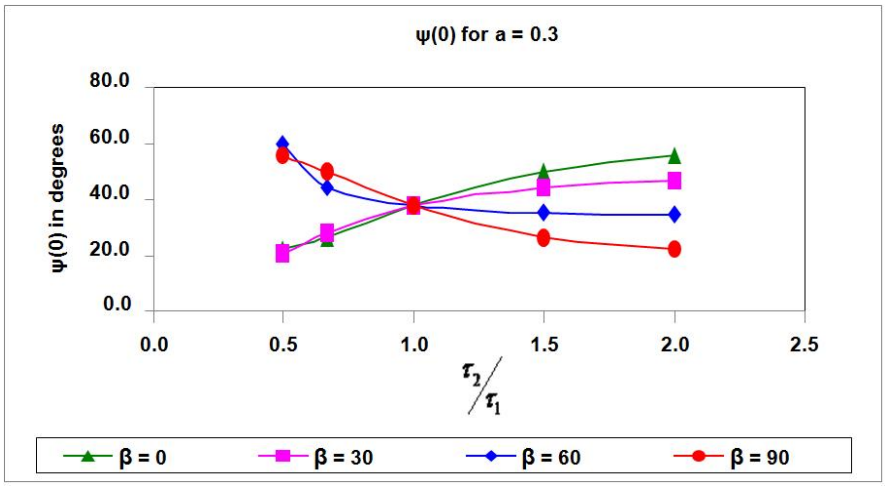

Figure 27: Plot showing the variation of ψ(0) for a = 0.3 (τ_{ave} = 300 and τ_2/τ_1 = 0.5, 0.67 ,1, 1.5, 2)

Figure 28 and 29 shows the variation of dimensionless moment with respect ratio of τ_2/τ_1 . Dimensionless moment is equal to the reciprocal of the dimensionless radius of curvature. Hence ψ' increases with increasing ratio of shear stress for smaller values of β. For $\tau_2/\tau_1 < 1$ there is an increase in the dimensionless moment with increasing β stating that orientation of atoms between the nanotube and substrate is more favourable for bending for higher values of β. On the other hand for $\tau_2/\tau_1 > 1$ the dimensionless moment decreases with increasing β stating that shear stress offered by the substrate is less and hence less bending. Sensitivity also decreases for higher values of β.

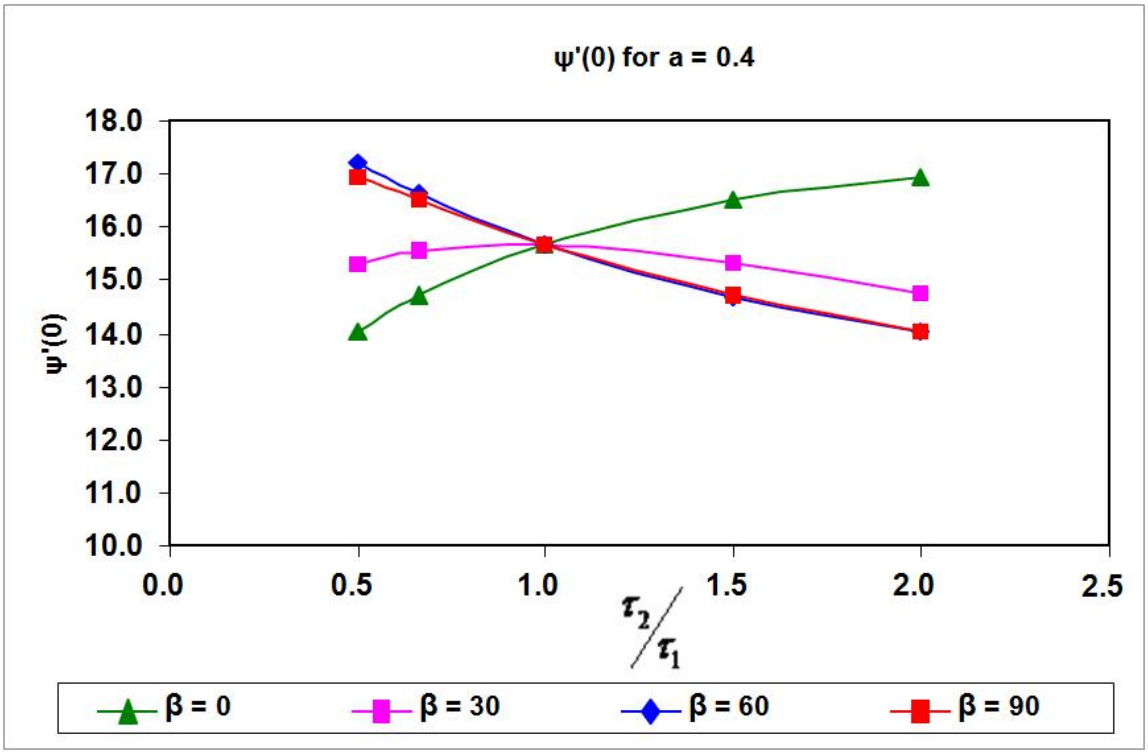

Figure 28: Plot showing the variation of ψ'(0) for a = 0.4 (τ_{ave} = 300 and τ_2/τ_1 = 0.5, 0.67 ,1, 1.5, 2)

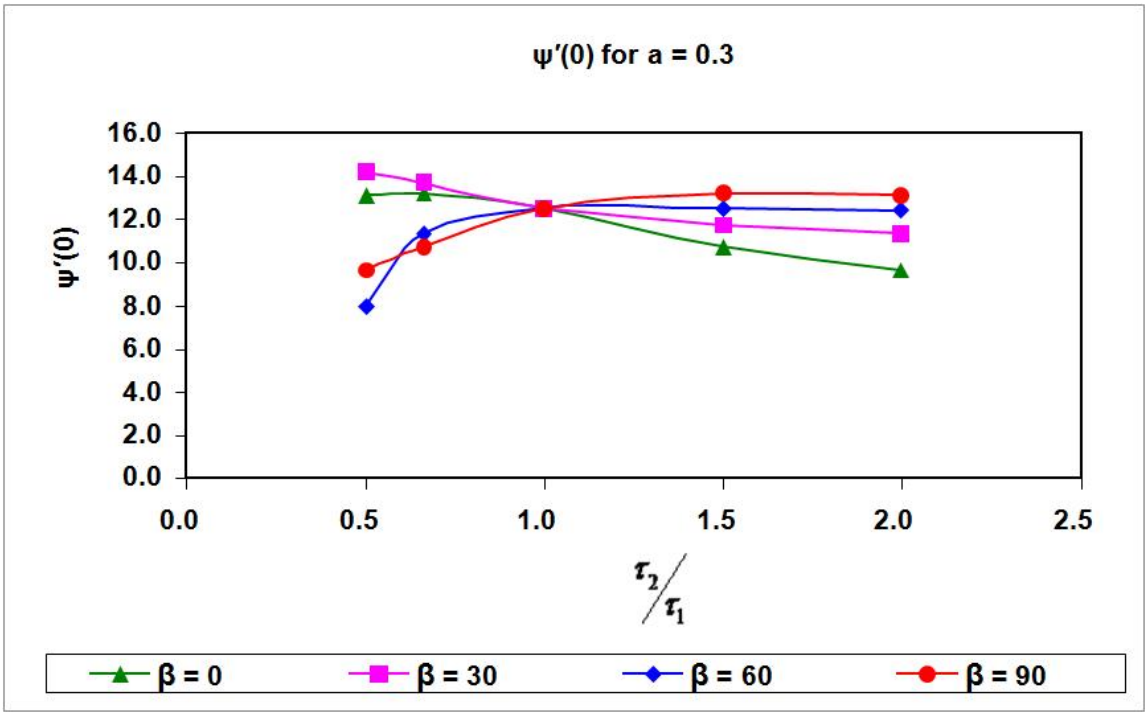

Figure 29: Plot showing the variation of ψ'(0) for a = 0.3 (τ_{ave} = 300 and τ_2/τ_1 = 0.5, 0.67 ,1, 1.5, 2)

Figure 30-33 show that the rotation angles at the ends of the beam vary almost in a similar manner for the non-symmetric cases of a = 0.4 and a = 0.3. For the extreme case of β= 90^0 the angle of rotation at either ends of the beam decreases with an increase in shear stress ratio and vice versa for other cases of β shown. As the shear stress ratio decreases for the applied load the right end of the CNT rotates through an angle which tends to 90^0. But on the left end of CNT there is a transition from negative to positive angles as the ratio increases. If there is a increase in shear stress for the applied load there is less bending of nanotube and hence less angle of rotation at either ends of CNT.

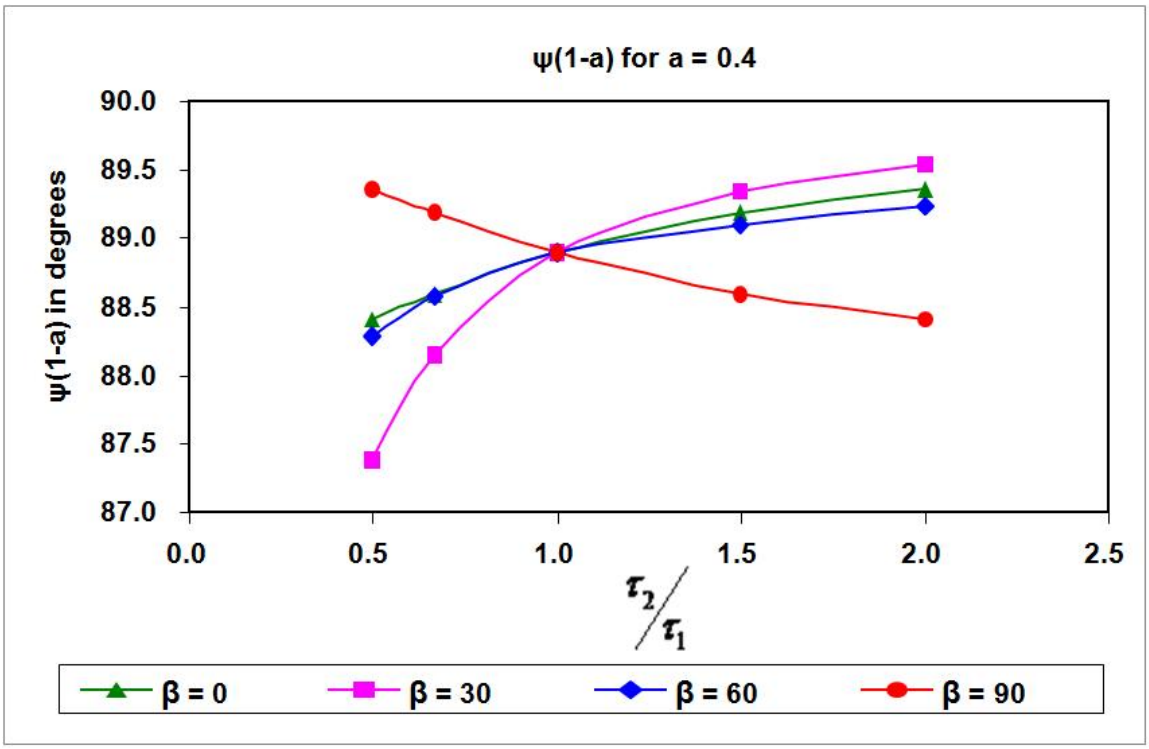

Figure 30: Plot showing the variation of ψ(1-a) for a = 0.4 (τ_{ave} = 300 and τ_2/τ_1 = 0.5, 0.67 ,1, 1.5, 2)

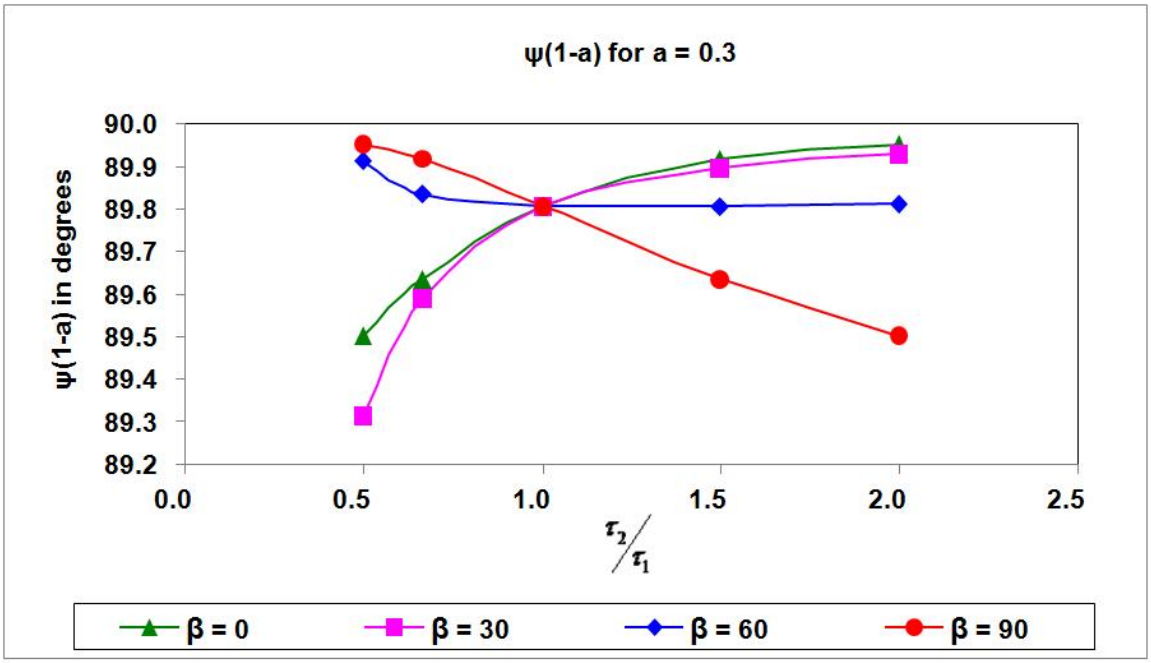

Figure 31: Plot showing the variation of ψ(1-a) for a = 0.3 (τ_{ave} = 300 and τ_2/τ_1 = 0.5, 0.67 ,1, 1.5, 2).

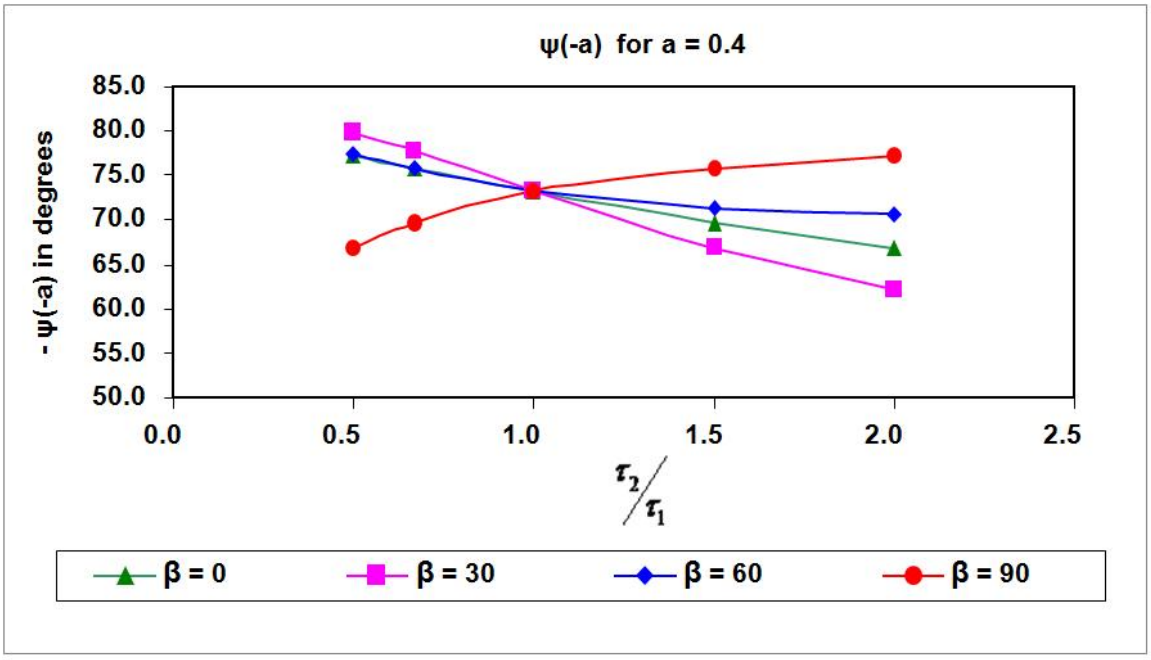

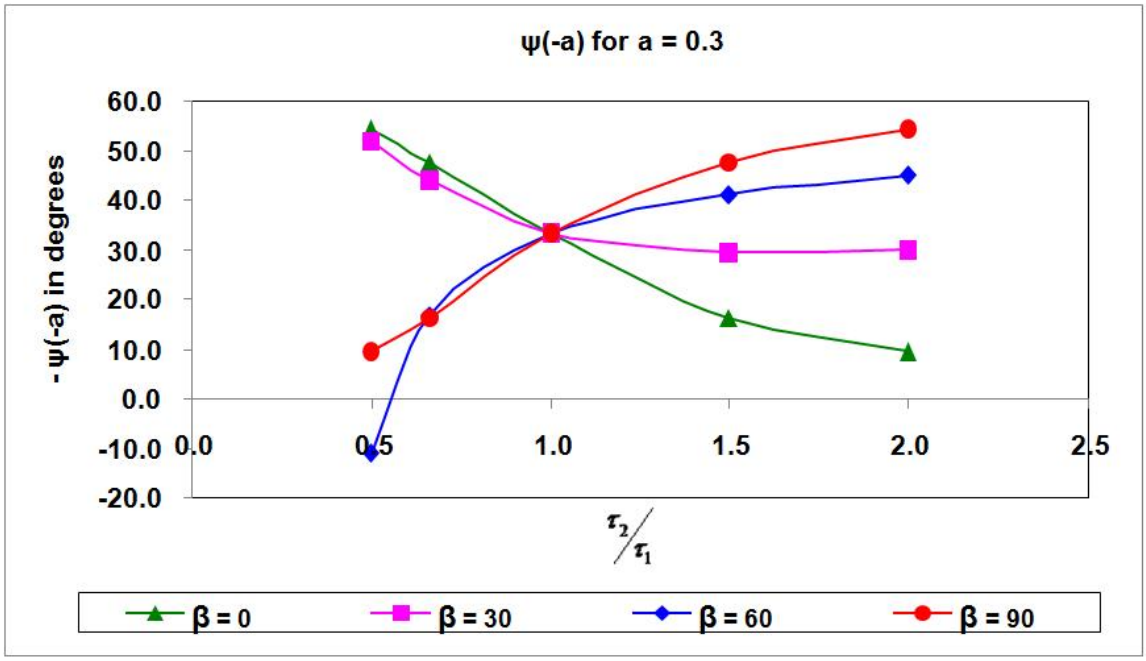

Figure 32, 33: Plot showing the variation of ψ(-a) for a = 0.4 and ψ(-a) for a = 0.3 respectively (τ_{ave} = 300 and τ_2/τ_1 = 0.5, 0.67 ,1, 1.5, 2)

By knowing the rotation angle at every cooridnate along the CNT and using numerical integration methods final deformed shape of the nanotube can be determined.The final shape of the nanotube for a constant value of β and varying τ_2/τ_1 is shown below. The nanotubes are plotted for a constant value of $\tau_{ave} = 300$.

Figures 34 and 35 shows the final shape of the CNT for a = 0.4 and a = 0.3 and for various values of β and a constant value of $\tau_{ave} = 300$.Smaller friction leads to a straight tube in the direction of travel while larger friction produces a bent configuration. For the cases discussed below all cases produces a bent equilibrium shape of the CNT.

For the case of $\beta = 0^0$ and 2 different values of a = 0.4 and 0.3 the longer end that is the right side beam bends through a larger angle as compared to the left beam. As the orientation of the nanotube is horizontal τ_1 plays a major role in determining the shear stress. The value of τ_1 is a direct measure of the shear stress offered by the substrate. As the value of τ_1 decrease there is more bending of nanotube. As the point of application of the load moves away from the midpoint the accuracy of finding the shear stress from deformed shape of nanotube increases. For the other extreme case of $\beta = 90^0$ the effect of τ_2 is more since the nanotube is placed in the vertical direction with respect to substrate.

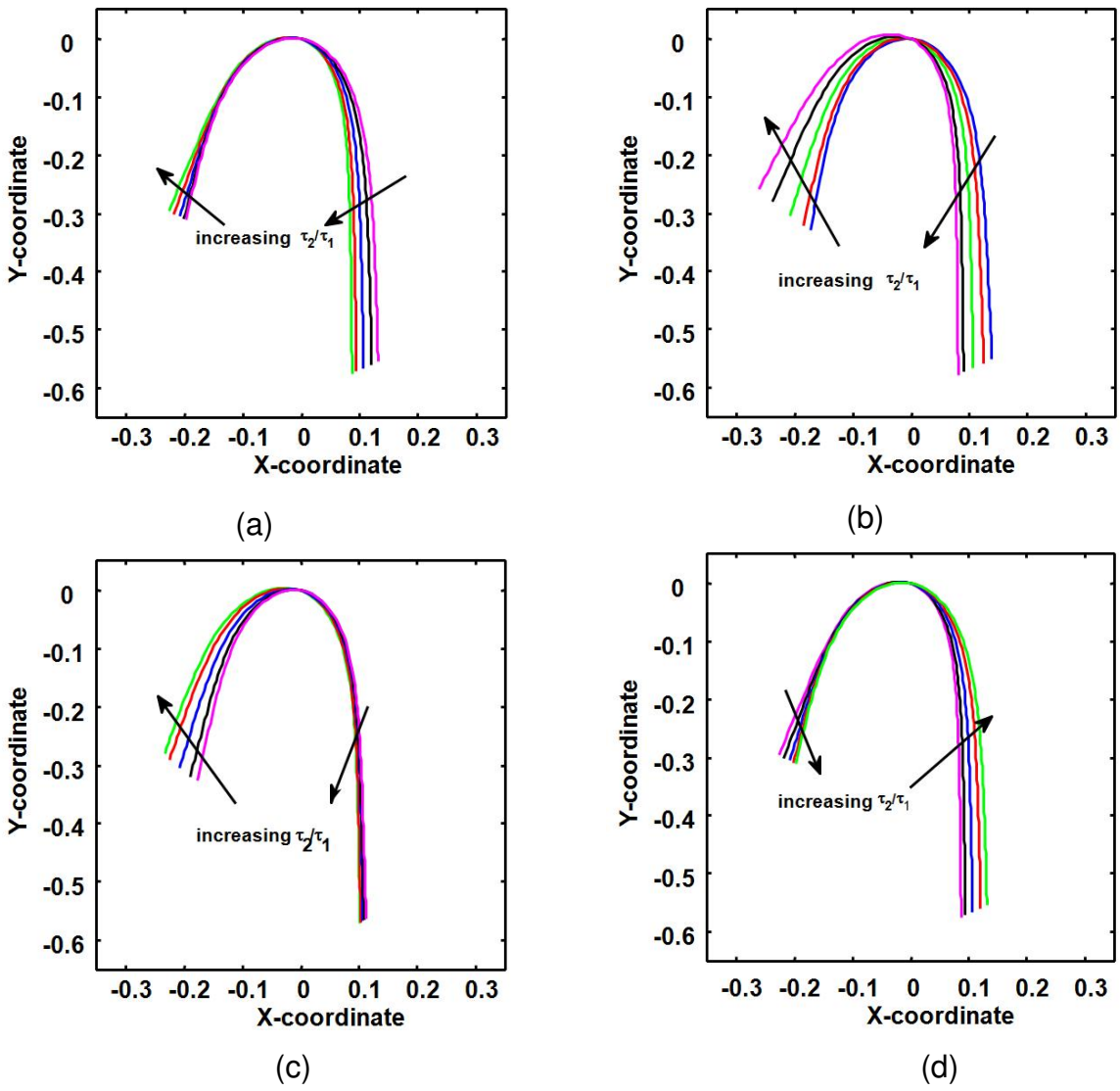

Figure 34: Final shape of CNT for a = 0.4 (τ_{ave} = 300 and τ_2/τ_1 = 0.5, 0.67 ,1, 1.5, 2) (a) β = 0^0 , (b) β = 30^0 ,(c) β = 60^0 ,(d) β = 90^0

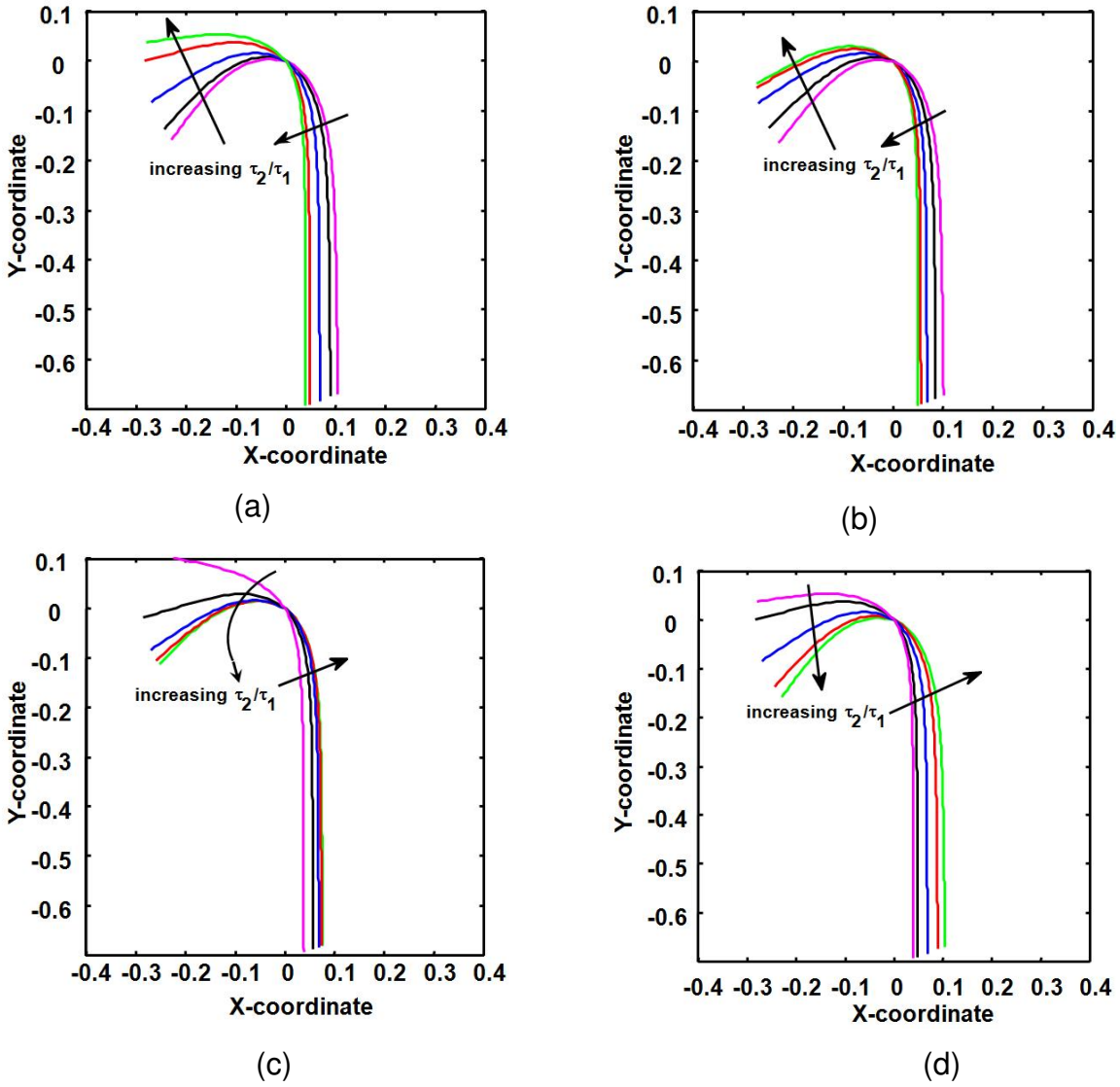

Figure 35: Final shape of CNT for a = 0.3 (τ_{ave} = 300 and τ_2/τ_1 = 0.5, 0.67 ,1, 1.5, 2) (a) β = 0^0 , (b) β = 30^0 ,(c) β = 60^0 ,(d) β = 90^0

Conclusion:

A simple method to determine the frictional interaction between a CNT and substrate using an AFM has been analyzed to determine its feasibility. Modeling has demonstrated that this technique is practical to use for a variety of CNT diameters and lengths, provided the aspect ratio is within a range of approximately 100-250 which depends weakly on the frictional interaction. For high values of the frictional interaction there is insufficient change in the final shape of the CNT to accurately resolve the shear stress. For low values of the frictional interaction the tube may roll rather than slide. Results are best if the AFM tip is placed somewhat away from the midpoint of CNT before dragging. However if the value of "*a*" is too small, then the tube can slip off of the AFM tip. The advantage of this technique is its simplicity. It does not require calibration of the AFM cantilever stiffness, as the force that the AFM exerts is not measured. For the same reason any force due to frictional interaction between the AFM tip and the substrate also does not affect the accuracy of the measurement.

The method utilized for the isotropic substrate is extended to find the results for an anisotropic substrate. This analysis gives information about the orientation of nanotube with respect to substrate and explains the effect of changing the angle of inclination. The configuration of the interlocking carbon atoms are the essential source of friction at atomic level. Changing the orientation of the nanotube changes the atomic configuration and hence the friction. Results are best fit if the AFM tip is placed a bit away from the midpoint of the CNT. The simulation is limited to a series of τ_{ave} values where the solution converges for the given equations. Sensitivity also becomes a issue for higher values of shear stress average (τ_{ave}).

REFERENCES

1. S. Iljima (1991). “Helical microtubles of graphitic carbon,” *Nature*, vol. 354, pp. 56-58.

2. T. Hertel, R. Martel, and P. Avouris (1997). “Manipulation of individual carbon nanotubes and their interaction with surfaces,” *Journal of Physical Chemistry B,* vol. 102, pp. 910-915.

3. M.R. Falvo, G. Clary, A. Helser, S. Paulson, R.M. Taylor II, V. Chi, F. P. Brooks Jr, S. Washburn, and R. Superfine (1998). “Nanomanipulation experiments exploring frictional and mechanical properties of carbon nanotubes,” *Microscopy and Microanalysis,* vol. 4, pp. 504-512.

4. M.R. Falvo, R.M. Taylor II, A. Helser, V. Chi, F.P. Brooks, S. Washburn and R. Superfine (1999). “Nanometer-scale rolling and sliding of carbon nanotubes,” *Nature*, vol. 397, pp. 236-238.

5. U.D. Schwarz, O. Zwörner, P. Köster, and R. Wiesendanger (1997). “Quantitative analysis of the frictional properties of solid materials at low loads. I. Carbon compounds,” *Physical Review B,* vol. 56, pp. 6987-6996.

6. M.R. Falvo, J. Steele, R.M. Taylor II and R. Superfine (2000). “Evidence of commensurate contact and rolling motion: AFM manipulation studies of carbon nanotubes on HOPG,” *Tribology Letters,* vol. 9, pp. 73-76.

7. M.R. Falvo and R. Superfine (2000). “Mechanics and friction at the nanometer scale,” *Journal of Nanoparticle Research,* vol. 2, pp. 237-248.

8. K. Miura, M. Ishikawa, R. Kitanishi, M. Yoshimura , K. Ueda, Y. Tatsumi, and N. Minami (2001). “Bundle structure and sliding of single-walled carbon nanotubes observed by frictional-force microscopy,” *Applied Physics Letters,* vol. 78, pp. 832-834.

9. J.D. Whittaker, E.D. Minot, D.M. Tanenbaum, P.L. McEuen and R.C. Davis (2006). “Measurement of adhesion force between carbon nanotubes and a silicon dioxide substrate” Nano Letters, vol. 6, pp. 953-957.

10. T. Hertel, R.E. Walkup, and P. Avouris (1998). “Deformation of carbon nanotubes by surface van der Waals forces,” *Physical Review B,* vol. 58, pp. 13,870-13,873.

11. A. Pantano, D.M. Parks, and M.C. Boyce (2004). “Mechanics of deformation of single- and multi-wall carbon nanotubes,” *Journal of the Mechanics and Physics of Solids,* vol. 52, pp. 789-821.

12. A. Buldum and J.P. Lu (1999). “Atomic scale sliding and rolling of carbon nanotubes,” *Physical Review Letters,* vol. 83, pp. 5050-5053.

13. M. Cheng and Y. Lu (2006). “Friction between carbon nanotube and graphite using molecular dynamics,” *IEEE Conference on Emerging Technologies – Nanoelectronics* – Proceedings, pp. 169-172.

14. R. Frisch-Fay (1962). *Flexible Bars.* Butterworths & Co., London.

15. Y. Nakayama (2007). “Plasticity of carbon nanotubes: Aiming at their use in nanosized devices,” *Japanese Journal of Applied Physics,* vol. 46, pp. 5005-5014.

Appendix A

A.1 : MATLAB program for Symmetric condition

Code 1:

```
%program for symmetric condition to find psi(0.1) psi(0.2)and psi(0.5)
clear all
clc
global p
p = 1;                  %value of dimensionless load
coord=1;                %variable used for continuous plot and not as single points
while (p <= 600)
lspan =  [0,0.1,0.2,0.5];
low = 0;
high = 25;
z0 = [0 (low+high)/2];
[s1,z] = ode23('symmetry',lspan,z0);        %solving ODE
x = length (s1);                            %finding length of s1
while ((z(x,2)*10000000 >= 1) || (z(x,2)*10000000 <= -1))
                                            %while loop for condition psi'(0.5)=0

   if z(x,2)>0
      high = (low+high)/2;
   else
      low = (low+high)/2;
   end
   z0 = [0 (low+high)/2];
   [s1,z] = ode23('symmetry',lspan,z0);
    x = length (s1);
end
   [s1,z] = ode23('symmetry',lspan,z0);
   c=p;
```

```
    datax(coord) = 6657.0978*c*1e-6;          %calculating shear stress from P
    datay(coord) = z(2,1)* (180/pi);          %conversion of psi(0.1) to degrees
    dataz(coord) = z(3,1)* (180/pi);          %conversion of psi(0.2) to degrees
    dataw(coord) = z(x,1)* (180/pi);          %conversion of psi(0.5) to degrees

if p==1
    p=p+9;
else
p=p+10;
end
coord=coord+1;
end;
figure(1)
plot(datax,datay,'LineWidth',3)                    % Plot of psi(0.1) vs shear stress
hold on
plot(datax,dataz,'LineWidth',3)                    % Plot of psi(0.2) vs shear stress
hold on
plot(datax,dataw,'LineWidth',3)                    % Plot of psi(0.5) vs shear stress
hold on
```

Code 2:

Program calls a function by name symmetry.

```
function zdot  = symmetry(s1,z)          % function symmetry used for solving ODE
global p
zdot = [z(2);(-p*(0.5-s1)*cos(z(1)))];    % z(1) is psi and z(2) is psi'
end
```

Code 3:

```
%program for symmetric condition  to find the variation of R vs shear
clear all
clc
global p
p = 100;                % high value of P to get a clear view on least values of R
coord = 1;              %  variable used for continuous plot and not as single points
while (p <= 600)
lspan =  [0 0.5];      %length of CNT
low = 0;
high = 25;
z0 = [0 (low+high)/2];
[s1,z] = ode23('symmetry',lspan,z0);                    %solving ODE
x = length (s1);                                        %finding length of s1
while ((z(x,2)*10000000 >= 1) || (z(x,2)*10000000 <= -1))
                                                %while loop for condition psi'(0.5)=0

   if z(x,2)>0
      high = (low+high)/2;
   else
      low = (low+high)/2;
   end
   z0 = [0 (low+high)/2];
   [s1,z] = ode23('symmetry',lspan,z0);
    x = length (s1);
end
   [s1,z] = ode23('symmetry',lspan,z0);
    c=p;
    D(coord) = 6657.0978*c*1e-6;            %calculating shear stress from P
    B = z(x,1)*(180/pi);                    %output of psi(0.5)
    A(coord) = z(1,2) ;                     %output of psi'(0)
```

```
    L = 300;                                %length of nanotube
    R(coord) = (L/A(coord));                %radius of curvature
if p==10
   p=p+40;
else
p=p+20;
end
coord = coord+1;
end;
plot(D,R)
```

A-2 : **MATLAB program for Non-symmetric condition**

Code 1:

```
% program showing variation of psi(0),psi'(0),psi(-a) and psi(1-a) vs shear stress
clear all
clc
global P                %assigning value for dimensionless constant P
P = 400;
global a                %assigning value for length 'a'
a = 0.4;
global s11              %assigning length for beam from 0 to (1-a)
s11 = [0 (1-a)];
global s22              %assigning length for beam from 0 to -a
s22 = [0 -a];
global dataC            %variable for plotting psi(1-a)
global dataD            %variable for plotting psi(-a)
global X                %variable assigned to P dimensionless load
npts = 150;
Ps = linspace(400,0,npts);          %varying load
z0 = [0.2 19];      %initial guess for psi(0) and psi'(0)
global coord       %variable plotting as continuous plots and not as discrete points
 coord = 1;
for i = 1:npts
     P = Ps(i);
  dataT(coord) = 6657.0978*P*1e-6;
                      %conversion of shear stress from dimensionless load
  B = fsolve(@beam,z0);             %solving both equations
  z0 =  B;
  dataE(coord) = B(1)*(180/pi);      %storing psi(0) as an array
  dataF(coord) = B(2);               %storing psi'(0) as an array
  coord = coord + 1;
end
```

```
figure(1)
plot(dataT,dataE,'k');   %plot for shear stress and psi(0)
hold on
figure(2)
plot(dataT,dataF,'k') ;  %plot for shear stress and psi'(0)
hold on
figure(3)
plot(dataT,dataC,'k') ;  %plot for shear stress and psi(1-a)
hold on
figure(4)
plot(dataT,dataD,'k') ; %plot for shear stress and psi(-a)
hold on
```

Code 2:

```
function A = beam(z0)
global s11 s22 P dataC dataD X coord
X = P;
 [s1,z] = ode23('myfun1',s11,z0);      %ode23 for s1>0
%indicating output of ode for s1>0
x = length(s1);                        %number of outputs
A(1) = z(x,2);                         %Moment(1-a)
dataC(coord) = z(x,1)*(180/pi);        %psi(1-a) conversion in degrees
 [s2,z] = ode23('myfun',s22,z0);       %ode23 for s2<0
%indicating output of ode for s1<0
 y = length(s2);                       %number of outputs
 A (2) = z(y,2);                       %Moment(-a)
dataD(coord) = -z(y,1)*(180/pi);       %psi(-a) conversion in degrees
```

Code 3:

```
function y1 = myfun1(s1,z)
                                % ODE solving for right side beam (length from 0 to 1-a)
global P a
y1 = [z(2); (-P*((1-a)*cos(z(1))))+(P*(s1*cos(z(1))))];
                                 %z(1)  is psi and z(2) is psi'
end

function y2 = myfun(s2,z)
                               % ODE solving for left side beam (length from -a to 0)
global P a
y2 =[z(2) ; ((P*a*cos(z(1)))+(P*(s2*cos(z(1)))))];
                                 %z(1)  is psi and z(2) is psi'
end
```

Code 4:

```
% program for finding the shape in non symmetric condition
clear all
clc
global P          %assigning value for dimensionless constant P
P = 300;
global a          %specifying value of a distance from right end of the the beam
a = 0.4;
global del        %small length considered as del
del = 0.005;
global s11        %assigning length for beam from 0 to (1-a)
s11 = [0:del:(1-a)];  %length for right side beam
global s22              %assigning length for beam from 0 to -a
s22 = [0:-del: -a];     %length for left side beam
z0 = [0.265 15.6742];     %guess for psi0 = e and psip0 = f
B = fsolve(@beam,z0)   %solving for correct values of psi(0) and psi'(0)
```

```
[s1,z] = ode23('myfun1',s11,B)     %numerical integration part for right side beam
x = length(s1)                     %number of output
del = 0.005;                %least length division on either side of beam for analysis
XX(1) = 0;
YY(1) =  0;
psi(1) = z(1,1);
F(1) = cos(psi(1));
G(1) = -sin(psi(1));
dataX(1) = 0;
dataY(1) = 0;
coord = 2;                         %variable for continuous plot
for i = 3:2:x                      % for loop for final shape of right side beam
  psi(i-1) = z(i-1,1);
  psi(i) = z(i,1);
  F(i-1) = cos(psi(i-1));
  F(i) = cos(psi(i));
  G(i) = -sin(psi(i));
  G(i-1) = -sin(psi(i-1));
  XX(i) = (0.005/3)*(F(i-2)+(4*F(i-1))+F(i))+ XX(i-2);
  YY(i) = (0.005/3)*(G(i-2)+(4*G(i-1))+G(i))+ YY(i-2);
  dataX(coord) = XX(i);
  dataY(coord) = YY(i);
  coord = coord+1;
end
plot(dataX,dataY,'m')              %plot showing final shape of right side beam
  axis tight square;
  hold on
[s2,z] = ode23('myfun',s22,B)      %numerical integration part for left side beam
y = length(s2);
del = -0.005;
XX(1) = 0;
```

```
YY(1) =  0;
psi(1) = z(1,1);
F(1) = cos(psi(1));
G(1) = sin(psi(1));
coordi = 2;                          %variable for continuous plot
for i = 3:2:y                        %for loop for final shape for left side beam
  psi(i-1) = z(i-1,1);
  psi(i) = z(i,1);
  F(i-1) = cos(psi(i-1));
  F(i) = cos(psi(i));
  G(i) = -sin(psi(i));
  G(i-1) = -sin(psi(i-1));
  XX(i) = (del/3)*(F(i-2)+(4*F(i-1))+F(i))+ XX(i-2);
  YY(i) = (del/3)*(G(i-2)+(4*G(i-1))+G(i))+ YY(i-2);
  dataXX(coordi) = XX(i);
  dataYY(coordi) = YY(i);
  coordi = coordi+1;
 end
plot(dataXX,dataYY,'m')              %plot showing the final shape for left side beam
  axis tight square;
  hold on
```

A- 3 : **MATLAB program for anisotropic substrate**

Code 1:

```
%program to find the final shape of nanotube for various orientation angle
clear all
clc
d = 1.3e-9;             %diameter of CNT
b = 0.6*d;              %interaction width of CNT
L = 300e-9;             %length of CNT
E = 1e9;                %young's modulus of CNT
I = (pi/64)*(d^4);      %Second moment of cross-sectional area
global a s11 s22 shear1 shear2 t1 t2 beta del
a = 0.5;                %length at which load is applied
del = 0.005;            %length of individual division
s11 = 0:del:(1-a);      %length of CNT on right side beam
s22 = 0:-del:-a;        %length of CNT on left side beam
t1 = 300;               %shear stress when CNT is parallel to horizontal direction
t2 = 300;               %shear stress when CNT is parallel to vertical direction
tave = (t1+t2)/2;       %shear stress average
angle = 0;              %orientation angle beta in degrees
beta = (pi/180)*angle;       %orientation angle beta in radians
shear1 =  -150;              %initial guess for shear force on right side beam
shear2 =   150;              %initial guess for shear force on left side beam
z0 = [-0 16];           %initial guess for rotation angle and moment at loading point
B = fsolve(@beam,z0)      %command for non-linear equation solving
[s1,z] = ode23('myfun1',s11,B);     %ode solving for right side beam
x = length(s1);                     %number of outputs
A(1) = z(x,2);                      %moment at (1-a)
psi(1) = z(1,1);                    %angle at the first point
F(1) = cos(2*(psi(1)+beta));
XX(1) = ((t1-t2)/2)*F(1)*del;       %second term in shear stress integration
  for i = 3:2:x
```

```
   psi(i-1) = z(i-1,1);
   psi(i) = z(i,1);
   F(i-1) = cos(2*(psi(i-1)+beta));
   F(i) = cos(2*(psi(i)+beta));
   XX(i) = ((t1-t2)/2)*(del/3)*(F(i-2)+(4*F(i-1))+F(i))+ XX(i-2);
   end
X = XX(i);
YY = ((t1+t2)/2)*(1-a);                %first term in shear stress integration
shear3 = -X-YY                         %calculated shear force
diff = abs(shear3-shear1)              %check for convergence for shear1
[s2,z] = ode23('myfun',s22,B);         %ode solving for left side beam
y = length(s2);                        %number of outputs
psi(1) = z(1,1);                       %angle at first point
A(2) =  z(y,2);
F(1) = cos(2*(psi(1)+beta));
AA(1) = ((t1-t2)/2)*F(1)*del;
      for j = 3:2:y
   psi(j-1) = z(j-1,1);
   psi(j) = z(j,1);
   F(j-1) = cos(2*(psi(j-1)+beta));
   F(j) = cos(2*(psi(j)+beta));
   AA(j) = ((t1-t2)/2)*(del/3)*(F(j-2)+(4*F(j-1))+F(j))+ AA(j-2);
      end
Y = AA(j);                             %second term in shear stress integration
BB = ((t1+t2)/2)*a;                    %first term in shear stress integration
shear4 = Y+BB                          %shear force for left side beam
diff1 = abs(shear4-shear2)             %check for convergence for shear2
while (diff>1e-4*tave || diff1>1e-4*tave)
                                       %check for convergence for both sides of the beam
```

```
if (diff>1e-4*tave )
   shear1 =  shear3;              %updating with new shear force value for right side
beam
end
if (diff1>1e-4*tave )
   shear2 = shear4;              %updating with new shear force value for left side
beam
end
B = fsolve(@beam,z0)
        %same steps from 23-64 followed with updated value of shear force guess
[s1,z] = ode23('myfun1',s11,B);
x = length(s1);
A(1) = z(x,2);
psi(1) = z(1,1);
F(1) = cos(2*(psi(1)+beta));
XX(1) = ((t1-t2)/2)*F(1)*del;
  for i = 3:2:x
  psi(i-1) = z(i-1,1);
  psi(i) = z(i,1);
  F(i-1) = cos(2*(psi(i-1)+beta));
  F(i) = cos(2*(psi(i)+beta));
  XX(i) = ((t1-t2)/2)*(del/3)*(F(i-2)+(4*F(i-1))+F(i))+ XX(i-2);
  end
X = XX(i);
YY = ((t1+t2)/2)*(1-a);
shear3 = -X-YY
diff = abs(shear3-shear1)
[s2,z] = ode23('myfun',s22,B);
y = length(s2);
psi(1) = z(1,1);
A(2) =  z(y,2);
```

```
F(1) = cos(2*(psi(1)+beta));
AA(1) = ((t1-t2)/2)*F(1)*del;
      for j = 3:2:y
  psi(j-1) = z(j-1,1);
  psi(j) = z(j,1);
  F(j-1) = cos(2*(psi(j-1)+beta));
  F(j) = cos(2*(psi(j)+beta));
  AA(j) = ((t1-t2)/2)*(del/3)*(F(j-2)+(4*F(j-1))+F(j))+ AA(j-2);
     end
Y = AA(j);
BB = ((t1+t2)/2)*a;
shear4 = Y+BB
diff1 = abs(shear4-shear2)
end
 [s1,z] = ode23('myfun1',s11,B)  %solving for final shape of CNT for right side
beam
   X(1) = 0;
Y(1) =  0;
psi(1) = z(1,1);
F(1) = cos(psi(1));
G(1) = -sin(psi(1));
dataX(1) = 0;
dataY(1) = 0;
coord = 2;    %variable to get a continuous plot
              for i = 3:2:x
  psi(i-1) = z(i-1,1);
  psi(i) = z(i,1);
  F(i-1) = cos(psi(i-1));
  F(i) = cos(psi(i));
  G(i) = -sin(psi(i));
  G(i-1) = -sin(psi(i-1));
```

```
  X(i) = (0.005/3)*(F(i-2)+(4*F(i-1))+F(i))+ X(i-2);
  Y(i) = (0.005/3)*(G(i-2)+(4*G(i-1))+G(i))+ Y(i-2);
  dataX(coord) = X(i);
  dataY(coord) = Y(i);
  coord = coord+1;
            end
plot(dataX,dataY,'m')          %plot showing final shape of right side beam
  axis tight square;
  hold on
[s2,z] = ode23('myfun',s22,B)      %solving for final shape of CNT for left side
beam
X(1) = 0;
Y(1) =  0;
psi(1) = z(1,1);
F(1) = cos(psi(1));
G(1) = sin(psi(1));
coordi = 2;      %variable to get a continuous plot
               for i = 3:2:y
  psi(i-1) = z(i-1,1);
  psi(i) = z(i,1);
  F(i-1) = cos(psi(i-1));
  F(i) = cos(psi(i));
  G(i) = -sin(psi(i));
  G(i-1) = -sin(psi(i-1));
  X(i) = (-del/3)*(F(i-2)+(4*F(i-1))+F(i))+ X(i-2);
  Y(i) = (-del/3)*(G(i-2)+(4*G(i-1))+G(i))+ Y(i-2);
  dataXX(coordi) = X(i);
  dataYY(coordi) = Y(i);
  coordi = coordi+1;
               end
 plot(dataXX,dataYY,'m')       %plot showing the final shape for left side beam
```

```
  axis tight square;
  hold on
```

Code 2:

```
function A = beam (z0)
global s11 s22 a  dataC dataD coord x y
 [s1,z] = ode23('myfun1',s11,z0);   %ode23 for s1>0
                                    %indicating output of ode for s1>0
x = length(s1);                     %number of outputs
A(1) = z(x,2);                      %Moment(1-a)
dataC(coord) = z(x,1)*(180/pi);     %psi(1-a) conversion in degrees
 [s2,z] = ode23('myfun',s22,z0);     %ode23 for s2<0
                                     %indicating output of ode for s1<0
 y = length(s2);                     %number of outputs
 A (2) = z(y,2);                     %Moment(-a)
dataD(coord) = -z(y,1)*(180/pi);     %psi(-a) conversion in degrees
```

Code 3:

```
function y1 = myfun1(s1,z)
                          % ODE solving for right side beam (length from 0 to 1-a)
global shear1 shear2  a t1 t2 beta s11 s22
y1 = [z(2); (shear1+(((t1+t2)/2)+(((t1-t2)/2)*cos(2*(z(1)+beta))))*s1)*cos(z(1))];
                          %z(1)  is psi and z(2) is psi'
end

function y2 = myfun(s2,z)
                           % ODE solving for left side beam (length from -a to 0)
global shear1 shear2 a t1 t2 beta s11 s22
y2 =[z(2) ; (shear2+(((t1+t2)/2)+(((t1-t2)/2)*cos(2*(z(1)+beta))))*s2)*cos(z(1))];
                           %z(1)  is psi and z(2) is psi'
end
```

Code 4:

```
%program for varying shear stress average
clear all
clc
d = 1.3e-9;                    %diameter of CNT
b = 0.6*d;                     %interaction width of CNT
L = 300e-9;                    %length of CNT
E = 1e9;                       %young's modulus of CNT
I = (pi/64)*(d^4);             %Second moment of cross-sectional area
global a s11 s22 shear1 shear2 t1 t2 beta del dataC dataD coord
a = 0.5;                       %length at which load is applied
coord = 1;                     %variable for continuous plot
del = 0.005;                   %length of individual division
s11 = 0:del:(1-a);             %length of CNT on right side beam
s22 = 0:-del:-a;               %length of CNT on left side beam
npts = 100;                    %number of divisions of shear stress average
t = linspace(300,100,npts); %linearly spaced shear stress average values
 z0 = [0 17];        %initial guess for rotation angle and moment at loading point
for i = 1:npts
angle = 0;                      %orientation angle beta in degrees
beta = (pi/180)*angle;          %orientation angle beta in radians
x = 1.5;                       %ratio of shear stress (t2/t1)
  tave = t(i)                  %shear stress average
  t1 = (2*tave)/(1+x);  %calculation of shear stress when CNT is parallel to X-axis
  t2 = (x*t1);             %calculation of shear stress when CNT is parallel to Y-axis
         if tave==300  %initial values of shear force to start with
shear1 =  -170;
shear2 =   170;
         else
      shear1 = shear3;
      shear2 = shear4;
```

```
        end
         B = fsolve(@beam,z0)            %solving non-linear equations
         z0 = B;                         %updating the initial guess
        [s1,z] = ode23('myfun1',s11,B); %ode solving for right side beam
        x = length(s1);                  %number of outputs
        A(1) = z(x,2);                   %moment at (1-a)
        psi(1) = z(1,1);                 %angle at the first point
        F(1) = cos(2*(psi(1)+beta));
        XX(1) = ((t1-t2)/2)*F(1)*del;    %second term in shear stress integration
      for i = 3:2:x
psi(i-1) = z(i-1,1);
psi(i) = z(i,1);
F(i-1) = cos(2*(psi(i-1)+beta));
F(i) = cos(2*(psi(i)+beta));
XX(i) = ((t1-t2)/2)*(del/3)*(F(i-2)+(4*F(i-1))+F(i))+ XX(i-2);
      end
          X = XX(i);
          YY = ((t1+t2)/2)*(1-a);         %first term in shear stress integration
          shear3 = -X-YY;                 %calculated shear force
          diff = abs(shear3-shear1);      %check for convergence for shear1
          [s2,z] = ode23('myfun',s22,B); %ode solving for left side beam
          y = length(s2);                 %number of outputs
          psi(1) = z(1,1);                %angle at first point
          A(2) =  z(y,2);
          F(1) = cos(2*(psi(1)+beta));
          AA(1) = ((t1-t2)/2)*F(1)*del;
       for j = 3:2:y
psi(j-1) = z(j-1,1);
psi(j) = z(j,1);
F(j-1) = cos(2*(psi(j-1)+beta));
F(j) = cos(2*(psi(j)+beta));
```

```
AA(j) = ((t1-t2)/2)*(del/3)*(F(j-2)+(4*F(j-1))+F(j))+ AA(j-2);
      end
         Y = AA(j);                    %second term in shear stress integration
         BB = ((t1+t2)/2)*a;           %first term in shear stress integration
         shear4 = Y+BB;                %shear force for left side beam
         diff1 = abs(shear4-shear2);   %check for convergence for shear2
         while (diff>1e-4*tave || diff1>1e-4*tave)
                                %check for convergence for both sides of the beam
           if (diff>1e-4*tave )
              shear1 =  shear3;
                       %updating with new shear force value for right side beam
           end
           if (diff1>1e-4*tave )
              shear2 = shear4;
                      %updating with new shear force value for left side beam
           end
           B = fsolve(@beam,z0)
     %same steps from 32-74 followed with updated value of shear force guess
           [s1,z] = ode23('myfun1',s11,B);
           x = length(s1);
           A(1) = z(x,2);
           psi(1) = z(1,1);
           F(1) = cos(2*(psi(1)+beta));
           XX(1) = ((t1-t2)/2)*F(1)*del;
             for i = 3:2:x
             psi(i-1) = z(i-1,1);
             psi(i) = z(i,1);
             F(i-1) = cos(2*(psi(i-1)+beta));
             F(i) = cos(2*(psi(i)+beta));
             XX(i) = ((t1-t2)/2)*(del/3)*(F(i-2)+(4*F(i-1))+F(i))+ XX(i-2);
             end
```

```
            X = XX(i);
            YY = ((t1+t2)/2)*(1-a);
            shear3 = -X-YY;
            diff = abs(shear3-shear1)
            [s2,z] = ode23('myfun',s22,B);
            y = length(s2);
            psi(1) = z(1,1);
            A(2) =  z(y,2);
            F(1) = cos(2*(psi(1)+beta));
            AA(1) = ((t1-t2)/2)*F(1)*del;
                  for j = 3:2:y
              psi(j-1) = z(j-1,1);
              psi(j) = z(j,1);
              F(j-1) = cos(2*(psi(j-1)+beta));
              F(j) = cos(2*(psi(j)+beta));
              AA(j) = ((t1-t2)/2)*(del/3)*(F(j-2)+(4*F(j-1))+F(j))+ AA(j-2);
                 end
            Y = AA(j);
            BB = ((t1+t2)/2)*a;
            shear4 = Y+BB;
            diff1 = abs(shear4-shear2);
          end
        shear1 = shear3;
        shear2 = shear4;
         z0 = B;                          %final value after solving non-linear equation
         dataE(coord) = B(1)*(180/pi) ;
                                          %angle of rotation at loading point in degrees
           dataF(coord) = B(2);       %moment at the loading point
          coord = coord+1;

end
```

```
figure(1)
plot (t,dataE,'g')                %angle of rotation at loading point
hold on
figure(2)
plot (t,dataF,'g')                %moment at loading point
hold on
figure(3)
plot (t,dataC,'g')                %psi(1-a) plot
hold on
figure(4)
plot (t,dataD,'g')                %psi(-a) plot
hold on
```